Quantifying Measurement Uncertainties of MIT Research Reactor's New Digital Nuclear Safety System

by

Rachel Parus

SUBMITTED TO THE DEPARTMENT OF NUCLEAR SCIENCE AND ENGINEERING IN PARTIAL FULFILLMENT OF THE REQUIREMENTS FOR THE DEGREE OF

BACHELOR OF SCIENCE IN NUCLEAR SCIENCE AND ENGINEERING

AT THE

MASSACHUSETTS INSTITUTE OF TECHNOLOGY

JUNE 2018

© 2018 Massachusetts Institute of Technology. All rights reserved.

Signature of Author:_____

Rachel Parus
Department of Nuclear Science and Engineering
May 18, 2018

Certified by:_____

Lin-wen Hu
Director, Research and Services Senior Research Scientist
Thesis Supervisor

Accepted by:_____

Michael Short
Assistant Professor of Nuclear Science and Engineering
Chairman, NSE Committee for Undergraduate Students

Quantifying Measurement Uncertainties of MIT Research Reactor's New Digital Nuclear Safety System

by

Rachel Parus

Submitted to the Department of Nuclear Science and Engineering on May 18, 2018 in Partial Fulfillment of the Requirements for the Degree of Bachelor of Science in Nuclear Science and Engineering

Abstract

Accurate measurement of reactor power is one of the most important requirements in order to ensure the reliable and safe operation of a nuclear reactor. The MIT research reactor, (MITR-II), currently has outdated analog reactor period and power monitoring instruments that are difficult to read and in need of frequent adjustment. Replacing these old monitors with digital ones is an important step in continuing to ensure MITR-II's reliable and safe operation. Four Mirion DWK 250's, wide-range neutron flux monitors that provides reactor period and power level monitoring, have been assembled and connected to the MITR for parallel testing. Before they can fully replace the existing analog monitors, the accuracy of measurement of the DWK's must be quantified to meet the performance requirements described in the Safety Analysis Report (SAR) and obtain Nuclear Regulatory Commission (NRC) approval. As part of the calibration tests, reactor power measured by the four DWK channels was recorded and compared to the reactor thermal power obtained through calorimetry calculations. The measurement uncertainties of the four DWK channels were quantified by taking into account the statistical uncertainties of data recorded over two separate operating periods in 1 minute intervals after thermal and xenon equilibrium were reached. The reactor neutron power measured by each channel was found to fit a normal distribution during steady-state operation, and the 3σ values, 99.7% confidence level, were found to be less than 1.6% of the average power detected for each DWK indicating each device's high level of precision. The average percent error between DWK and thermal power was determined to be 4% for each DWK, thus a thorough review of calibration procedures should be performed to ensure an accurate indication of reactor power. Furthermore, as the setpoints of the DWK's may be adjusted over the core cycle of the reactor, the relationship between shim blade height and DWK adjustment was also determined by parallel testing and modelling. The adjustment of each of the DWK's over a fuel cycle was found to be minimal.

Thesis Supervisor: Lin-wen Hu
Title: Director, Research and Services Senior Research Scientist

Acknowledgements

I would like to thank Dr. Lin-wen Hu, my thesis advisor, for all of her help in developing the thesis objectives and especially for her assistance in the results and discussion portions of the paper.

Thank you to Professor Michael Short for his edits and vital suggestions in improving the explanations and background portions especially.

I would also like to thank Akshay Dave for his support especially in the statistics and data analysis sections of the thesis. Thank you also to Dr. Kaichao Sun for the DWK modelling that was an essential part to the completion of the thesis objectives. I would like to thank the staff of the MITR-II reactor, namely Dane Kouttron, Director of Reactor Operations Al Quierolo, and Edward Lau for the help they provided especially towards the thesis completion.

I would also like to thank all of those that read and edited my thesis for clarity, my thesis is understandable because of you. Thank you to all of those in the NSE department, especially the faculty, administrators, and my fellow course-mates. The help and support I received from all of you was vital to the completion of my degree and this thesis.

Lastly, I would like to thank my friends and family especially for all of the support they have given me in the last four years. I would not be finishing this thesis today if it was not for their love!

Contents

1 Introduction **12**
1.1 Outdated Power Level Monitoring Systems in Reactors 12
1.2 Objectives 12

2 Background **14**
2.1 Description of the Current Period Monitoring System 14
2.2 Description of the Current Power Level Monitoring System 16
2.3 Scram Amplifier Operation 17
2.4 Current Power Level Monitoring System 17
2.5 DWK System Design 20

3 Methodology **23**
3.1 DWK Installation 23
3.2 Thermal Power Calculation 25
3.3 Convert DWK Detected Neutron Flux to Measured Reactor Power 26
3.4 Uncertainties of Thermal Power vs. DWK Power Measurements 26
3.5 Recorded Reactor Power Data 27
3.6 Statistical Analysis of Power Measurements 29
3.6.1 Modelling of Drift 30

4 Results and Discussion **31**
4.1 05-05-17 to 05-22-17 Statistics Quantification 31
4.2 10-13-17 to 12-19-17 Statistics Quantification 33
4.3 Fitted Normal Distributions 35
4.4 Average Percent Discrepancy 37
4.5 Quantifying DWK Drift 41
4.5.1 Modelling of Drift 44

5 Conclusion **46**
5.1 Statistical Measurement Uncertainties 46
5.2 Calibration of DWK's 46
5.3 DWK Adjustment Over an Operating Cycle 46

6 Suggestions for Future Work **47**

7 Appendix **48**

List of Figures

2.1 When a neutron is absorbed by the uranium coating of the fission chamber, a fission interaction occurs releasing two fission products that travel in nearly opposite directions. Whichever fission product cross over the fill gas of the detector will cause ionizations. 14

2.2 The operation of a fission chamber begins with the interaction between a neutron and the uranium coating of the inner cylinder. This creates a fission which produces fission products. These fission products ionize the gas between the inner and outer concentric tubes. The ionized particles are then moved by an electric current towards the inner tube. When the particles reach the inner tube, they create a current pulse which is sent to an external circuit that can be used as an indication of neutron flux in the reactor. The four new channels each have a fission chamber detector located in the core. 15

2.3 When a neutron is captured by the boron lining of an ion chamber, a lithium-7 atom, an alpha particle or helium-4 atom, and electrons are released. The alpha particle will then ionize the gas in the ion chamber. 15

2.4 The operation of an ion chamber begins with the capture of a neutron by the boron lining of the outer electrode. This capture releases an alpha particle or helium-4 atom that interacts with the fill gas of the ion chamber and ionizes particles due to the electric field created by the voltage that was applied across the outer and center electrodes. The electrons produced from this interaction move towards the center electrode. Once they reach this electrode, they are detected by the ion chamber and provide an indication of neutron flux. . . . 16

2.5 Scram amplifier faces for channels 4, 5, and 6. Each scram amplifier controls its associated channel and shim blade. Each safety amplifier has two dials. The left dial is used to set the scram setpoint at a value corresponding to 6.5 MW. The right dial is used to set the magnet current of the blade. These dials can be locked in at the desired setpoints. 18

2.6 The three meters of the scram amplifier are shown zoomed in. The first meter is used to set the level at which the reactor will scram if the input meter, in the middle, reaches that value. The right-most meter indicates the current being sent to the corresponding shim blade magnet for each channel. The maximum of the scram set meter is 50 however that level can correspond to a scram at < 6.5 MW. 19

2.7 A block diagram detailing the operation of the new nuclear safety system. The circuit begins from the leftmost side with the detector which measures neutron flux. The pre-amplifiers are downstream from the detectors and increase the voltage of the signals before they are sent to the digital displays in the control room. The associated scram responses are also detailed, namely the relationship with the withdraw permit circuit and shim blade magnets [8]. 21
2.8 The positions of each of the DWK fission chambers. DWK 1 is in 4IH3, DWK 2 is in 3GV2, DWK 3 is in 4IH1, and DWK 4 is in 3GV5. These are located around the core such that they provide adequate indication of the neutron flux in the reactor. 22

3.1 DWK's 1 and 2 installed in the instrumentation panel in the control room. The digital screen clearly and precisely indicates the level that is read by the DWK channels. The indication of the meter is precise. 23
3.2 DWK's 3 and 4 installed in the instrumentation panel in the control room. The setup for these is the same as DWK's 1 and 2. Clear, digital input display and precise meter indications. 24
3.3 The digital display of the neutron flux located on each of the four DWK installations. The scram points are set with a precise digital value. 25
3.4 Reactor power measured by DWK's 1-4 and thermal reactor power calculated from 05-05-17 to 05-22-17. Reactor power measurements were taken every minute from shutdown reactor power (0 MW) to full operation reactor power (5.7 MW) over approximately 17 days. The variation between the thermal reactor power and the DWK measured reactor power measured by each of the 4 DWK channels can be seen. 28
3.5 Reactor power measured by DWK's 1-4 compared to thermal reactor power. Reactor power measurements were taken every minute from shutdown reactor power (0 MW) to full operation reactor power (5.7 MW) over an entire operating period and fuel cycle of the reactor (approximately 67 days. The variation between the thermal reactor power and the DWK measured reactor power measured by each of the 4 DWK channels can be seen. 29

4.1 Reactor power measured by DWK's 1-4 during a startup on 05-05-2017 was plotted against the thermal power measured at the same time. R^2 tests for a linear regression model were then completed for each of the DWK channels to determine the linearity of the power increases detected by each channel. Each of the four channels was found to have an R^2 value that was greater than or equal to 0.9996, where $R^2 = 1$ indicates an exactly linear relationship between power increments. A $y = x$ line was included to show the variation in the slopes of each of the DWK channels when compared to thermal power. The slopes of the lines of each of the DWK channels when compared to thermal power appear to be different, likely due to their various locations around the core as seen in Figure 2.8. 33

4.2 The steady-state power detected by DWK 1 from minute 10000 to 30000 during the 10-13-17 to 12-19-17 operation period was grouped into energy power intervals of 0.01 MW from 5.42 MW to 5.56 MW (which correspond to the minimum and maximum 3σ values for DWK 1). Then a fitted normal distribution (depicted by the orange line) was plotted over the actual energy data using the mean and standard deviation of DWK 1. The normal distribution plotted shows the range of 99.7% of the DWK 1 power measurements. 35
4.3 The steady-state thermal power from minute 10000 to 30000 during the 10-13-17 to 12-19-17 operation period was grouped into energy power intervals of 0.02 MW from 5.6 MW to 5.86 MW (which correspond to the minimum and maximum 3σ values for thermal power over this range). Then a fitted normal distribution (depicted by the orange line) was plotted over the actual energy data using the mean and standard deviation of thermal power. The normal distribution plotted shows the range of 99.7% of the thermal power power measurements. 36
4.4 The fitted normal distributions for DWK 1 and thermal power were plotted using their means and standard deviations. The fitted normal distributions show the range of 99.7% of the DWK 1 and thermal power measurements respectively. The two fitted normal distributions do not intersect indicating there is likely an offset between the DWK channel calibration and actual thermal power. The spread of the thermal power is greater than that of the DWK indicating that the DWK detector is likely more precise. 37
4.5 Reactor power measured by DWK 1 from 10-13-2017 to 12-19-2017 was plotted against the thermal power measured at the same time. R^2 tests for a linear regression model were then completed for each of the DWK channels to determine the linearity of their relationship to thermal reactor power. DWK 1 was found to have $R^2 = 0.9984$. discrepancy lines at $\pm 5\%$ were included that show at steady-state operation, the majority of the data was within $\pm 5\%$ of the average. 39
4.6 Reactor power measured by DWK 2 from 10-13-2017 to 12-19-2017 was plotted against the thermal power measured at the same time. R^2 tests for a linear regression model were then completed for each of the DWK channels to determine the linearity of their relationship to thermal reactor power. DWK 2 was found to have $R^2 = 0.9984$. discrepancy lines at $\pm 5\%$ were included that show at steady-state operation, the majority of the data was within $\pm 5\%$ of the average. 39
4.7 Reactor power measured by DWK 3 from 10-13-2017 to 12-19-2017 was plotted against the thermal power measured at the same time. R^2 tests for a linear regression model were then completed for each of the DWK channels to determine the linearity of their relationship to thermal reactor power. DWK 3 was found to have $R^2 = 0.9988$. discrepancy lines at $\pm 5\%$ were included that show at steady-state operation, the majority of the data was within $\pm 5\%$ of the average. 40

4.8 Reactor power measured by DWK 4 from 10-13-2017 to 12-19-2017 was plotted against the thermal power measured at the same time. R^2 tests for a linear regression model were then completed for each of the DWK channels to determine the linearity of their relationship to thermal reactor power. DWK 4 was found to have $R^2 = 0.9993$. discrepancy lines at $\pm 5\%$ were included that show at steady-state operation, the majority of the data was within $\pm 5\%$ of the average. 40
4.9 The percent discrepancy between DWK 1 and thermal power during steady-state operation is plotted every ten minutes over 16 days from 09-09-17 to 09-25-17. This plot is overlaid with a black line representing the shim bank height over the same time frame. The percent discrepancy seems to drift downwards from day 8 to day 16. 41
4.10 The average percent discrepancy between each DWK and thermal power during steady-state operation was plotted at each shim bank height position over 16 days from 09-09-17 to 09-25-17. This plot is overlaid with a black line representing the shim bank height over the same time frame. There seems to be no trend in the change of average percent discrepancy over the operating period, as shim bank height increased. 42
4.11 The percent discrepancy between DWK 1 and thermal power during steady-state operation is plotted every ten minutes over 28 days from 10-16-17 to 11-13-17. This plot is overlaid with a black line representing the shim bank height over the same time frame. The percent discrepancy seems to drift downwards from day 15 to day 28. 43
4.12 The average percent discrepancy between each DWK and thermal power during steady-state operation was plotted at each shim bank height position over 28 days from 10-16-17 to 11-13-17. This plot is overlaid with a black line representing the shim bank height over the same time frame. There seems to be no trend in the change of average percent discrepancy over the operating period, as shim bank height increased. 44

7.1 The steady-state power detected by DWK 2 from minute 10000 to 30000 during the 10-13-17 to 12-19-17 operation period was grouped into energy power intervals of 0.01 MW from 5.49 MW to 5.62 MW (which correspond to the minimum and maximum 3σ values for DWK 2). Then a fitted normal distribution (depicted by the orange line) was plotted over the actual energy data using the mean and standard deviation of DWK 2. The normal distribution plotted shows the range of 99.7% of the DWK 2 power measurements. 48
7.2 The steady-state power detected by DWK 3 from minute 10000 to 30000 during the 10-13-17 to 12-19-17 operation period was grouped into energy power intervals of 0.02 MW from 5.415 MW to 5.615 MW (which correspond to the minimum and maximum 3σ values for DWK 3). Then a fitted normal distribution (depicted by the orange line) was plotted over the actual energy data using the mean and standard deviation of DWK 3. The normal distribution plotted shows the range of 99.7% of the DWK 3 power measurements. 49

7.3 The steady-state power detected by DWK 4 from minute 10000 to 30000 during the 10-13-17 to 12-19-17 operation period was grouped into energy power intervals of 0.02 MW from 5.38 MW to 5.6 MW (which correspond to the minimum and maximum 3σ values for DWK 4). Then a fitted normal distribution (depicted by the orange line) was plotted over the actual energy data using the mean and standard deviation of DWK 4. The normal distribution plotted shows the range of 99.7% of the DWK 4 power measurements. 49
7.4 The percent discrepancy between DWK 2 and thermal power during steady-state operation is plotted every ten minutes over 16 days from 09-09-17 to 09-25-17. This plot is overlaid with a black line representing the shim bank height over the same time frame. The percent discrepancy seems to drift downwards from day 8 to day 16. 50
7.5 The percent discrepancy between DWK 3 and thermal power during steady-state operation is plotted every ten minutes over 16 days from 09-09-17 to 09-25-17. This plot is overlaid with a black line representing the shim bank height over the same time frame. The percent discrepancy seems to drift downwards from day 8 to day 16. 50
7.6 The percent discrepancy between DWK 4 and thermal power during steady-state operation is plotted every ten minutes over 16 days from 09-09-17 to 09-25-17. This plot is overlaid with a black line representing the shim bank height over the same time frame. The percent discrepancy seems to drift downwards from day 8 to day 16. 51
7.7 The percent discrepancy between DWK 2 and thermal power during steady-state operation is plotted every ten minutes over 28 days from 10-16-17 to 11-13-17. This plot is overlaid with a black line representing the shim bank height over the same time frame. The percent discrepancy seems to drift downwards from day 15 to day 28. 51
7.8 The percent discrepancy between DWK 3 and thermal power during steady-state operation is plotted every ten minutes over 28 days from 10-16-17 to 11-13-17. This plot is overlaid with a black line representing the shim bank height over the same time frame. The percent discrepancy seems to drift downwards from day 15 to day 28. 52
7.9 The percent discrepancy between DWK 4 and thermal power during steady-state operation is plotted every ten minutes over 28 days from 10-16-17 to 11-13-17. This plot is overlaid with a black line representing the shim bank height over the same time frame. The percent discrepancy seems to drift downwards from day 15 to day 28. 52

List of Tables

4.1 Means, standard deviations, and 3-sigma values for steady-state operation from 8500 to 17500 minutes of the 05-05-17 to 05-22-17 DWK's 1-4 and thermal reactor power recording. The mean indicates the average power detected by each of the channels and the thermally calculated power. The standard deviation indicates the range ± the mean in which 66% of the data exists for each of the channels and the thermal power. The 3-sigma value indicates the range ± the mean in which 99.7% of the data exists for each of the channels and the thermal power. 31

4.2 99% confidence reactor power ranges for DWK's 1-4 and thermal power. This indicates that at steady-state operation of approximately 5.67 MW thermal reactor power, the power measured by any of the DWK's 1-4 or the power calculated using the thermal power will fall between their respective minimum and maximum reactor power levels with a 99.7% probability. The range of each of the 99.7% confidence intervals was divided by the mean reactor power for each DWK and thermal power. Each DWK has a 3σ range that is less than 2.7% of their respective means. The thermal power 3σ range is 3.11% of its mean, meaning it has a greater uncertainty than the DWK detectors. . . 32

4.3 Means, standard deviations, and 3σ values for steady-state operation of the 10-13-17 to 12-19-17 DWK's 1-4 and thermal reactor power recording. The mean indicates the average power detected by each of the channels and the thermally calculated power. The standard deviation indicates the range ± the mean in which 66% of the recorded power values exist for each channel and thermal power. The 3σ value indicates the range ± the mean in which 99.7% of the power values exist for each channel and thermal power. 34

4.4 99.7% confidence reactor power ranges for DWK's 1-4 and thermal tower. This indicates that at steady-state operation of approximately 5.67 MW thermal reactor power, the power measured by any of the DWK's 1-4 or the power calculated using the thermal power will fall between their respective minimum and maximum reactor power levels with a 99.7% likelihood. The range of each of the 99.7% confidence intervals was divided by the mean reactor power for each DWK's mean reactor power value. Each DWK has a 3σ range that is less than 2% of their respective means. The thermal power 3σ range is 4.12% of its mean, meaning it has a greater standard deviation than the DWK detectors. 34

4.5 The average percent discrepancies between each of the DWK channel measurements and the actual thermal reactor power during steady state operation of about 5.7 MW from 8500 to 13500 minutes from the 05-05-17 to 05-22-17 data (approximately 6.25 days) and from 10000 to 30000 minutes from the 10-13-17 to 12-19-17 data (approximately 13.8 days). For the 05-05-17 cycle, the average percent discrepancies were around 2% for DWK's 1, 2, and 3. DWK 4 had a percent discrepancy of 3.1%. For the 10-13-17 cycle, the average percent discrepancies were approximately 4% for DWK's 1, 3, and 4 and 3% for DWK 2. 38

Chapter 1

Introduction

1.1 Outdated Power Level Monitoring Systems in Reactors

Having accurate measurements of a nuclear reactor's operating conditions is necessary not only to meet Nuclear Regulatory Commission (NRC) requirements, but also to safely operate a reactor [1]. Reactor power monitoring is part of the reactor protection systems installed at every reactor in the United States and around the globe. However, many of the reactors in the United States were built in the 1950's and 60's; therefore, their reactor power level monitoring systems are becoming outdated [2], [3]. In order to continue to maintain safe reactor operation, comply with NRC regulations, and improve the reliability and accuracy of reactor power measurements, it is necessary to update these monitoring systems with state-of-the-art digital systems when feasible [4].

One of the reactors in the United States that has an aging power level monitoring system is the MITR-II research reactor at Massachusetts Institute of Technology (MIT). Since 2013, the Nuclear Reactor Laboratory (NRL) at MIT has been working to update the nuclear power level monitoring system. The reactor power level of the MITR and other research reactors is still monitored by an analog system. Several main components of the required period and power level monitoring devices are no longer available. The unreliability of this system has caused spurious scrams and unscheduled shutdown maintenance. Furthermore, one of the power level monitoring channels is out of commission, so an update is essential for continued reliable and safe reactor operation under NRC regulations. Replacing this analog system with a digital period and power level monitoring system is the next stage of advancement in reactor instrumentation. The MITR is one of the first research reactors in the U.S. working to license their digital power monitoring system.

1.2 Objectives

The goal of the MITR-II personnel is to replace the analog channel monitors with digital ones. However, prior to its full-scale replacement and implementation, the new digital monitoring system must be studied for accuracy in signals detected and calibration. Thus, in this work,

the reactor power measured by the newly installed DWK system at the MITR-II reactor will be compared to the actual thermal power of the reactor in order to determine the accuracy of each of the DWK channels.

This thesis project aims to determine the accuracy of the reactor power level readings of the new digital system. Specifically, there are three technical objectives for this study:

- Quantifying statistical measurement uncertainties of four DWK channels
- Calibrate DWK power measurements with reactor thermal power
- Analyze the effect of the shim bank height on digital system performance through a typical fuel cycle

The project will culminate in a technical report that outlines the statistical measurement uncertainties of the new digital monitoring system through analyzing data obtained from all 4 DWK channels that have undergone extensive testing. Furthermore, the power readings from these channels will be calibrated using reactor thermal power data obtained through calorimetry calculations. The effect of shim bank height on the detectors will be quantified during a fuel cycle that will form the basis of recommended adjustment range for these channels. This will inform the NRC of the new digital power level monitor's acceptability within regulations and will ideally provide more accurate and reliable reactor power measurements for the MITR-II.

Chapter 2

Background

2.1 Description of the Current Period Monitoring System

The MITR-II currently has three channels, (channels 1, 2, and 3) that are responsible for monitoring the reactor period. The reactor period provides an indication of the rate at which the power level is changing in the reactor. In order to operate the reactor, at least 2 out of 3 of the period channels have to be functioning. [5].

Channels 1 and 2 are comprised of a fission chamber and an uncompensated ion chamber, which are used to detect neutrons [6]. The fission chambers for channels 1 and 2 are used at low power levels because they are more sensitive to reactor period indications. During a reactor startup, the cables connecting channels 1 and 2 to their respective fission chambers must be pulled out and reinserted in order to switch from fission to ion chamber operation as the ion chambers come on-scale. Channel 3 has only an uncompensated boron-lined ion chamber and thus is not changed from a fission to an ion chamber during startup [6].

Fission chambers are comprised of two concentric tubes coated with highly enriched U-235. When a thermal neutron flies into the chamber and interacts with the uranium coating creating a fission, the fission products ionize the gas in the space between the inner and outer cylinders. The interaction that causes ionization of the gas is shown in Figure 2.1.

$$^{235}_{92}U + ^{1}_{0}n \rightarrow FP_1 + FP_2 + (2-3)^{1}_{0}n$$

$$FP_1 + fill\ gas \rightarrow e^- + \gamma$$

Figure 2.1: When a neutron is absorbed by the uranium coating of the fission chamber, a fission interaction occurs releasing two fission products that travel in nearly opposite directions. Whichever fission product cross over the fill gas of the detector will cause ionizations.

A small voltage source is applied to the chamber to create an electric field between the two tubes causing the ions and electrons to flow towards the middle electrode. When the

particles interact with the middle electrode, a current is produced that can be detected by an external detector circuit [6]. Fission chamber operation is shown in 2.2.

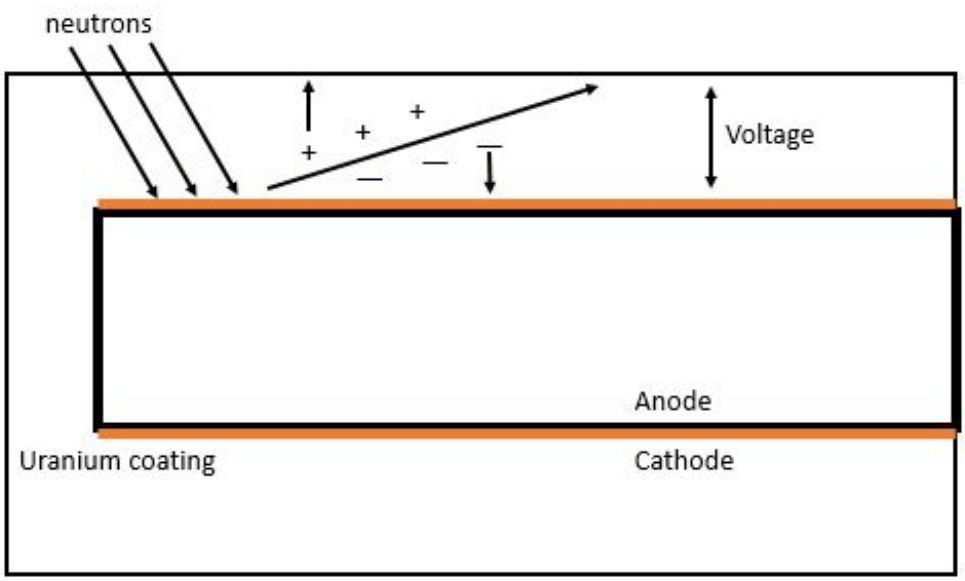

Figure 2.2: The operation of a fission chamber begins with the interaction between a neutron and the uranium coating of the inner cylinder. This creates a fission which produces fission products. These fission products ionize the gas between the inner and outer concentric tubes. The ionized particles are then moved by an electric current towards the inner tube. When the particles reach the inner tube, they create a current pulse which is sent to an external circuit that can be used as an indication of neutron flux in the reactor. The four new channels each have a fission chamber detector located in the core.

Ion chambers detect neutron flux when a particle of radiation interacts with the gas that fills the detector [6]. An electric field is created in the gas volume by applying a voltage potential across two electrodes over the detector [6]. Ion pairs are created between the electrodes. The electron will be attracted to the electrode that is positively charged (usually the center electrode) [6]. An electric current develops when either ion reaches their corresponding electrode. The current flow provides an indication of the neutron flux that the detector is receiving [6]. The outer electrode can be lined with boron in order to detect neutrons. A neutron will be captured by an atom of boron, emitting an alpha particle which then causes ionizations that will be detected by the center electrode [6]. The interaction that takes place between a neutron and the boron lining is shown in Figure 2.3.

$$^{10}_{5}B + ^{1}_{0}n \rightarrow ^{7}_{3}Li + ^{4}_{2}He + 5e^{-}$$

Figure 2.3: When a neutron is captured by the boron lining of an ion chamber, a lithium-7 atom, an alpha particle or helium-4 atom, and electrons are released. The alpha particle will then ionize the gas in the ion chamber.

A diagram of the operation of an uncompensated boron-lined ion chamber is shown in Figure 2.4.

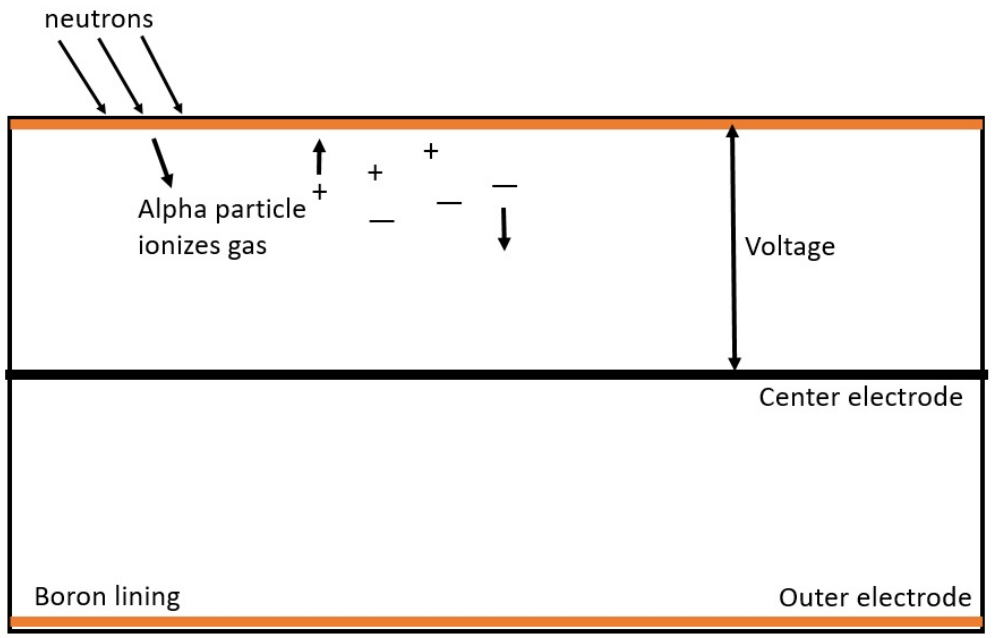

Figure 2.4: The operation of an ion chamber begins with the capture of a neutron by the boron lining of the outer electrode. This capture releases an alpha particle or helium-4 atom that interacts with the fill gas of the ion chamber and ionizes particles due to the electric field created by the voltage that was applied across the outer and center electrodes. The electrons produced from this interaction move towards the center electrode. Once they reach this electrode, they are detected by the ion chamber and provide an indication of neutron flux.

2.2 Description of the Current Power Level Monitoring System

The MITR-II currently has three channels, (4, 5, and 6) that are responsible for monitoring the thermal flux in the reactor [6]. The detectors in each of these channels are uncompensated boron-lined ion chambers. Two out of three of these channels must be operable in order to run the reactor. These channels have thermal neutron detectors located in the reflector region of the reactor. The neutron detectors are uncompensated boron-lined ion chambers. In order to display the thermal power detected by each of the channels, the DC current output of each channel's detector is sent to its associated scram amplifier which indicates the output of the current.

The thermal power of the MITR-II must not exceed 7.4 MW [5]. Thus, each scram amplifier is set to provide a reactor scram below that maximum value, at 6.5 MW [6]. The amplifier scram setpoint is determined and set on each channel's scram amplifier respectively, during the start-up checklist. Resetting the scram amplifier scram setpoint at the start of

each start-up compensates for burn-up of fuel in the reactor which requires adjustment of the scram-level setting on the amplifiers.

In addition to the high range amplifiers, there are also low range scram amplifiers that are installed into the channel 5 and 6 high range scram amplifier ports when operating at < 100 kW or when there is a procedure that requires work in the core tank [6]. These low range safety amplifiers are more sensitive than the high range amplifiers which permit them to provide more accurate thermal power indications at low power levels.

2.3 Scram Amplifier Operation

Each of the scram amplifiers is connected to a corresponding shim blade [6]. Shim blades are used to control the neutron flux in a reactor. Because shim blades are neutron absorbers, when they are fully inserted they absorb the neutrons required to sustain continued reactor operation and prevent further fission from occurring in the core, effectively shutting down the reactor. Thus, when the shim blades are pulled out of the core region, fewer neutrons are absorbed, neutron fission occurs within the fuel, and thermal power increases. Shim blades are held out of the reactor by a magnet [7]. Each shim blade has its own magnet that is connected to a scram amplifier. When the magnet is energized, the blade is held at the shim bank position, allowing the reactor to operate. If the magnet is de-energized, the corresponding blade will fall, resulting in the cessation of reactor operation.

The scram amplifiers are responsible for the energizing and de-energizing of the shim blade magnets. The positive DC input currents received by the channels 4, 5, and 6 scram amplifiers from each respective neutron detector are compared with the negative DC reference currents set by the scram setpoints [6]. When this differential current is positive, normal operation ensues and the amplifier sends a high-frequency AC source signal to an amplification and rectifying circuit which is used to energize the magnet of the corresponding shim blade [6]. If the differential current drops to zero, the field-effect transistor (FET), a device that controls current using an electric field, is shut off, resulting in the cessation of the AC signal sent to the corresponding shim blade magnet. This causes the magnet to de-energize and the corresponding shim blade to drop. Furthermore, the scram amplifiers are each connected to two scram relays. The first relay cuts off the power to its corresponding magnet power supply, resulting in the drop of a second shim blade (paired to maintain power balance in the core). The second relay causes the withdraw permit circuit to open. The withdraw permit circuit is responsible for permitting the movement of the shim blade drives and the energizing of their associated magnets [7]. Once the withdraw permit circuit is open, all of the remaining blades will drop as their magnets are de-energized.

2.4 Current Power Level Monitoring System

The current MITR-II channels are analog systems which are becoming increasingly outdated. Because the current power level monitors were installed in the 1970's, when parts of the scram amplifiers malfunction or break, there are limited replacement parts available to repair them. If parts to these old analog amplifiers were to become permanently unavailable, the reactor would be unable to run. The current MITR-II scram amplifier faces are shown in Figure 2.5.

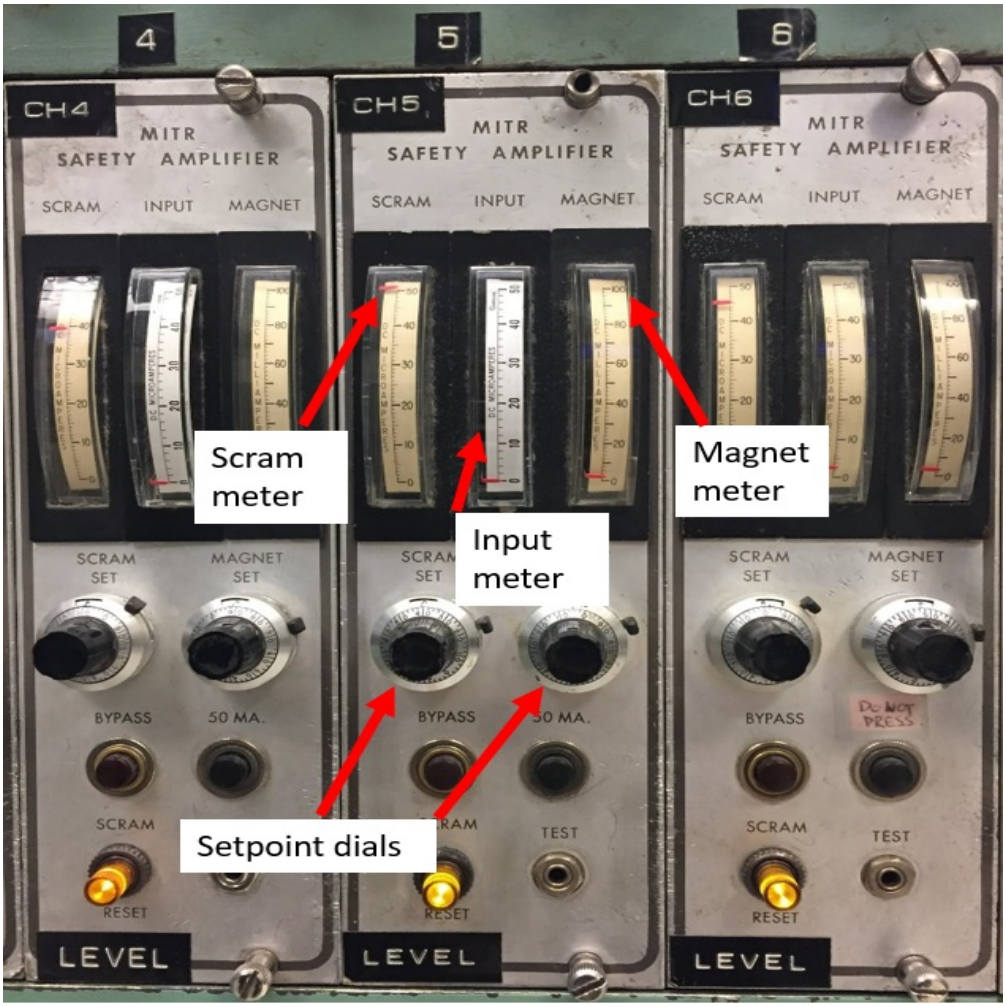

Figure 2.5: Scram amplifier faces for channels 4, 5, and 6. Each scram amplifier controls its associated channel and shim blade. Each safety amplifier has two dials. The left dial is used to set the scram setpoint at a value corresponding to 6.5 MW. The right dial is used to set the magnet current of the blade. These dials can be locked in at the desired setpoints.

Channels 1-6 each have their own associated scram amplifier. Throughout reactor operation, as the shim blades are moved as fuel depletes, the scram amplifiers have to be adjusted throughout the cycle of operation. There are three indications located on the scram amplifier face. The leftmost corresponds to the scram setpoint which is adjusted using the left dial during startups. The center meter corresponds to the input, which is what the channel reads as the neutron flux. The rightmost meter corresponds to the magnet current, or the strength of the current that is going to the associated shim blade. This is also set during a startup. In order to see better view the indications on the amplfier faces, Figure 2.6 shows a zoomed in image of the amplifier meters.

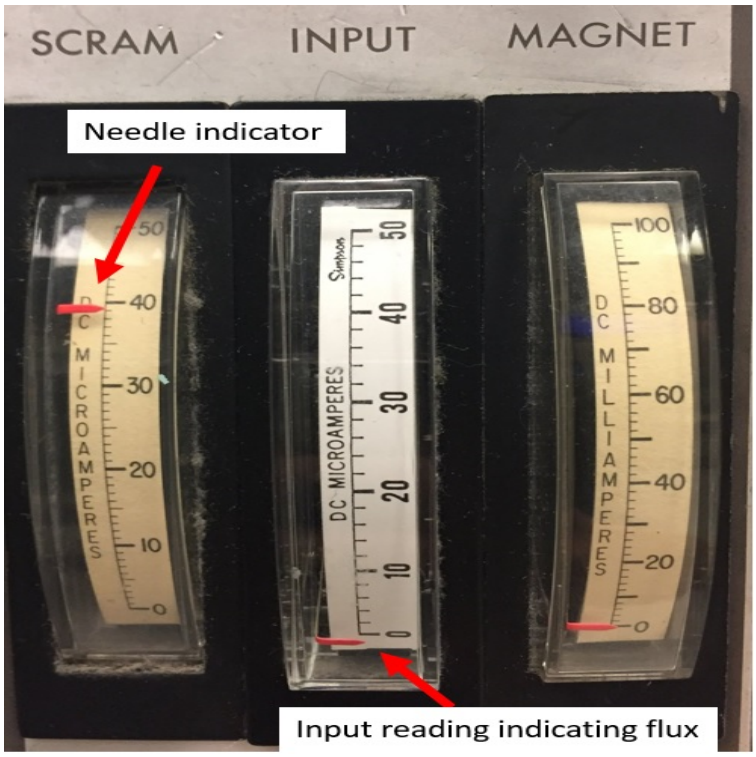

Figure 2.6: The three meters of the scram amplifier are shown zoomed in. The first meter is used to set the level at which the reactor will scram if the input meter, in the middle, reaches that value. The right-most meter indicates the current being sent to the corresponding shim blade magnet for each channel. The maximum of the scram set meter is 50 however that level can correspond to a scram at < 6.5 MW.

The high flux trip is set to provide a reactor scram when the detector output is equivalent to 6.5 MW, however the high flux scram set for 6.5 MW is often high off-scale (greater than the maximum value of 50) on the scram amplifiers. Thus, the actual power at which the reactor will scram is often less than the actual setpoint. This can result in spurious reactor scrams at power levels lower than 6.5 MW and unnecessary interruption of normal operation. The digital power level monitors will eliminate the uncertainty in the setting of the scram. Digital monitors have exact to the hundredth decimal place setpoints which permit them to be exactly accurate of the desired scram setpoint.

Technical specification requires that there are at least two operational thermal power level monitoring channels at all times[5]. This is intended to support that out of three channels, if only one reads a high flux level or malfunctions and the other two channels are still operational and in within the appropriate flux specifications, the reactor will not scram.

As explained above, as the MITR-II currently stands, the scram amplifiers for channels 5 and 6 must be switched out for low power monitoring whenever running at ¡ 100 kW start-ups [6]. In the new DWK design, there is no need for amplifier replacement when switching to operate at < 100 kW. Instead, there is a key switch that is turned to place the DWK system into < 100 kW mode, this automatically induces a scram if measured reactor power exceeds 100 kW during operation [8].

2.5 DWK System Design

The new DWK system is digital and is constructed of materials that have been produced in the last 25 years with an ensured Mirion vendor [8]. There are four DWK safety channels. Each of the channels is comprised of a wide-range fission chamber. Wide-range fission chambers can be used to detect neutron flux at source, intermediate, and full power ranges due to their ability to detect neutrons in various counting modes [9]. Each fission chamber is followed by a pre-amplifier. The pre-amplifier is used to increase the voltage of the incoming signal to reduce the effect of noise on the detected output [10]. Noise can be due to interactions with the center electrode tube from alpha particle interactions, for example. The pre-amplifier is also used to supply voltage to the fission chamber to create the electric field between the two concentric cylinders. Each pre-amplifier is followed by a neutron flux monitor, or a DWK. These DWK's monitor both reactor neutron flux (reactor power) and reactor period [8]. The DWK's receive and process the pre-amplifier's signal for neutron flux and reactor period. The DWK's are programmed to trip if flux exceeds 6.5 MW or if reactor period reaches 10 seconds [8]. These DWK's effectively replace each of the three period monitors (channels 1, 2, and 3) and each of the three neutron level monitors (channels 4, 5, and 6). A block diagram detailing the operation of the new nuclear saftey system is shown in Figure 2.7.

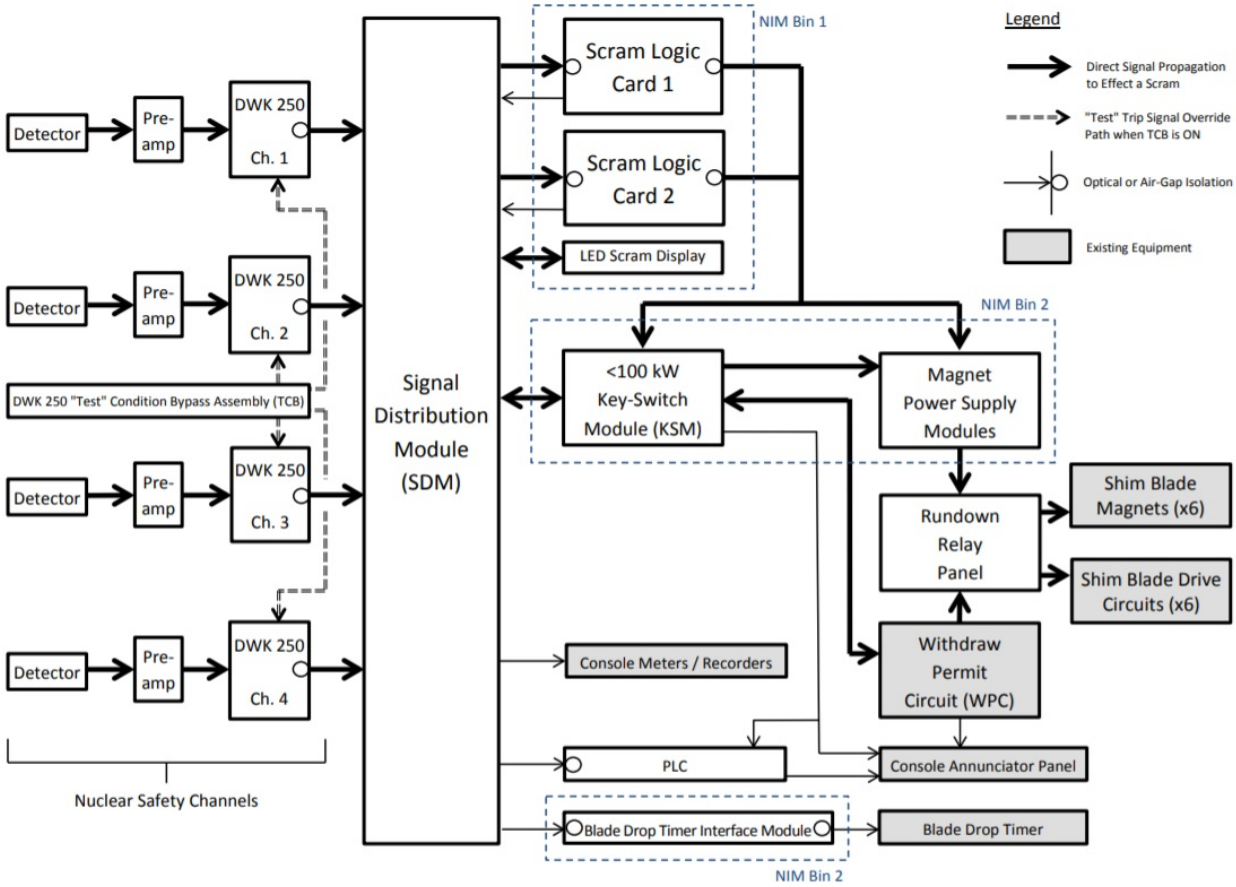

Figure 2.7: A block diagram detailing the operation of the new nuclear safety system. The circuit begins from the leftmost side with the detector which measures neutron flux. The pre-amplifiers are downstream from the detectors and increase the voltage of the signals before they are sent to the digital displays in the control room. The associated scram responses are also detailed, namely the relationship with the withdraw permit circuit and shim blade magnets [8].

In order to operate, there must be at least two out of four functional and operable DWK channels [8]. With four channels monitoring both period and power level, the DWK's bring on an added level of redundancy in the safety control of the reactor [8]. This increases the reliability of the safety systems of the reactor.

Each of the four DWK fission chambers is located within a different instrument port of the reactor. DWK channel 1 is located in horizontal instrument port, 4 inch internal diameter Instrument Horizontal port 3 (4IH3), DWK channel 2 is located in vertical instrument port, 3 inch internal diameter Graphite region Vertical port 2 (3GV2), DWK channel 3 is located in 4IH1 and DWK channel 4 is located in 3GV5 [8]. These were chosen in order to provide indication of flux and period in many parts of the core to get an accurate profile and because of their ideal accessibility. The locations of these in relation to the reactor core is shown in Figure 2.8.

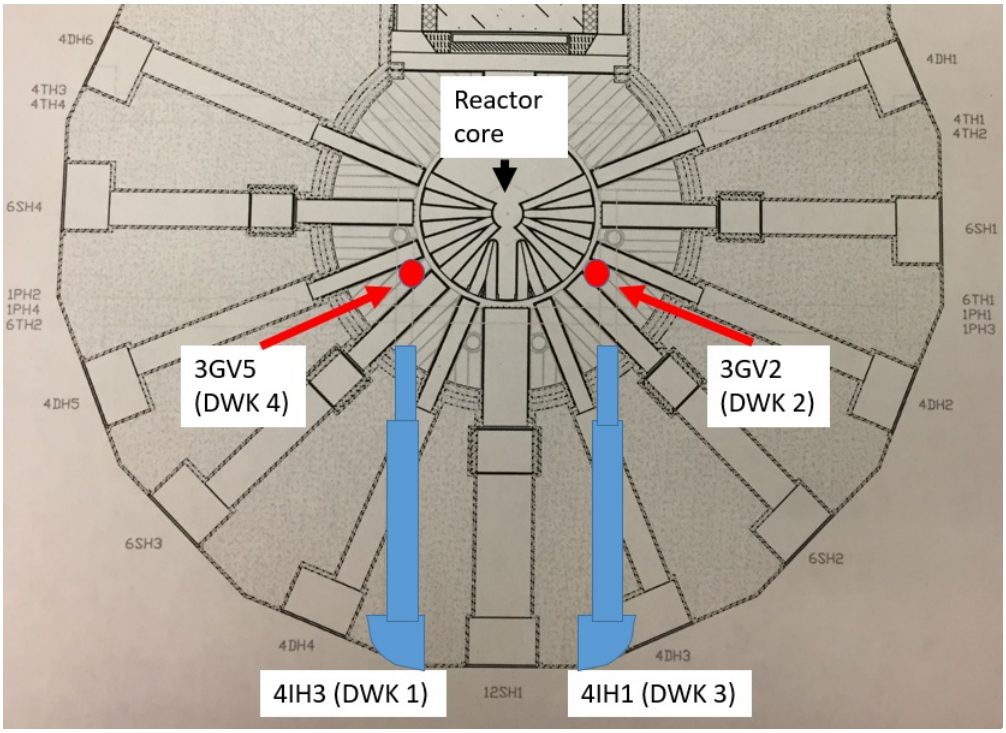

Figure 2.8: The positions of each of the DWK fission chambers. DWK 1 is in 4IH3, DWK 2 is in 3GV2, DWK 3 is in 4IH1, and DWK 4 is in 3GV5. These are located around the core such that they provide adequate indication of the neutron flux in the reactor.

From these positions, the DWK fission chambers and thus the channels can make readings of the reactor power in and around the core to provide indication to the reactor operator of the status of the reactor. Although these channels have been installed, prior to gaining Nuclear Regulatory Comission approval for their usage, they must prove to provide accurate indication of reactor power.

Chapter 3

Methodology

3.1 DWK Installation

In addition to being installed in the instrument ports of the reactor, the output screens for the four DWK power level monitoring channels were installed in the instrumentation panel of the MITR-II control room. Figures 3.1 and 3.2 show the faces of the four DWK channels.

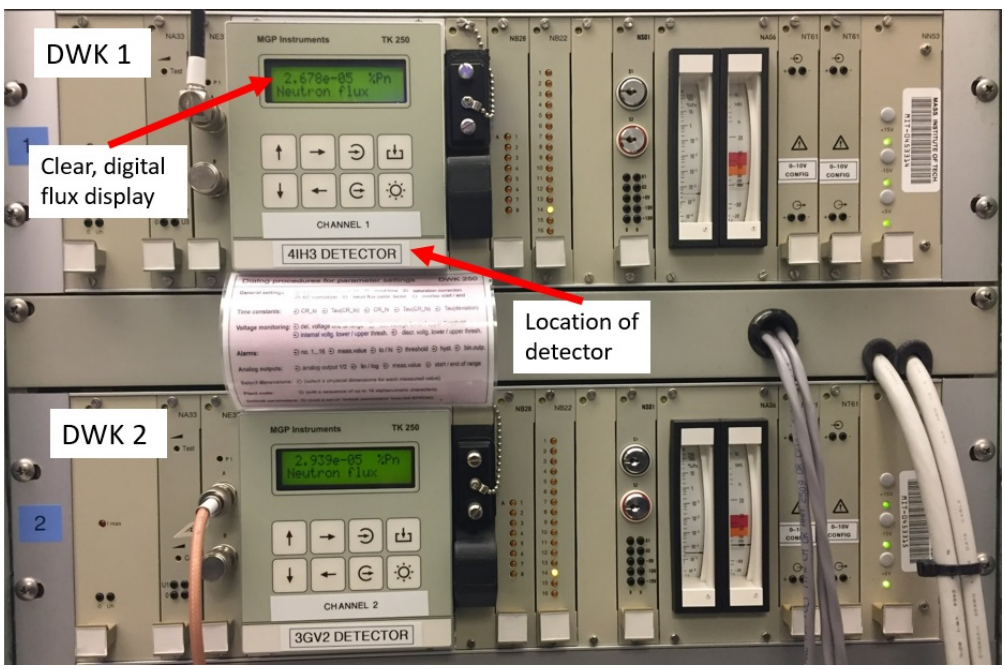

Figure 3.1: DWK's 1 and 2 installed in the instrumentation panel in the control room. The digital screen clearly and precisely indicates the level that is read by the DWK channels. The indication of the meter is precise.

Figure 3.2: DWK's 3 and 4 installed in the instrumentation panel in the control room. The setup for these is the same as DWK's 1 and 2. Clear, digital input display and precise meter indications.

The four DWK installations in the control room are the same. They have meters located on the right hand side with precise level indications due to the narrow needle. Each of the four DWK faces has a digital display of the neutron flux reading from the reactor located on the left hand side. This can be seen more clearly in Figure 3.3.

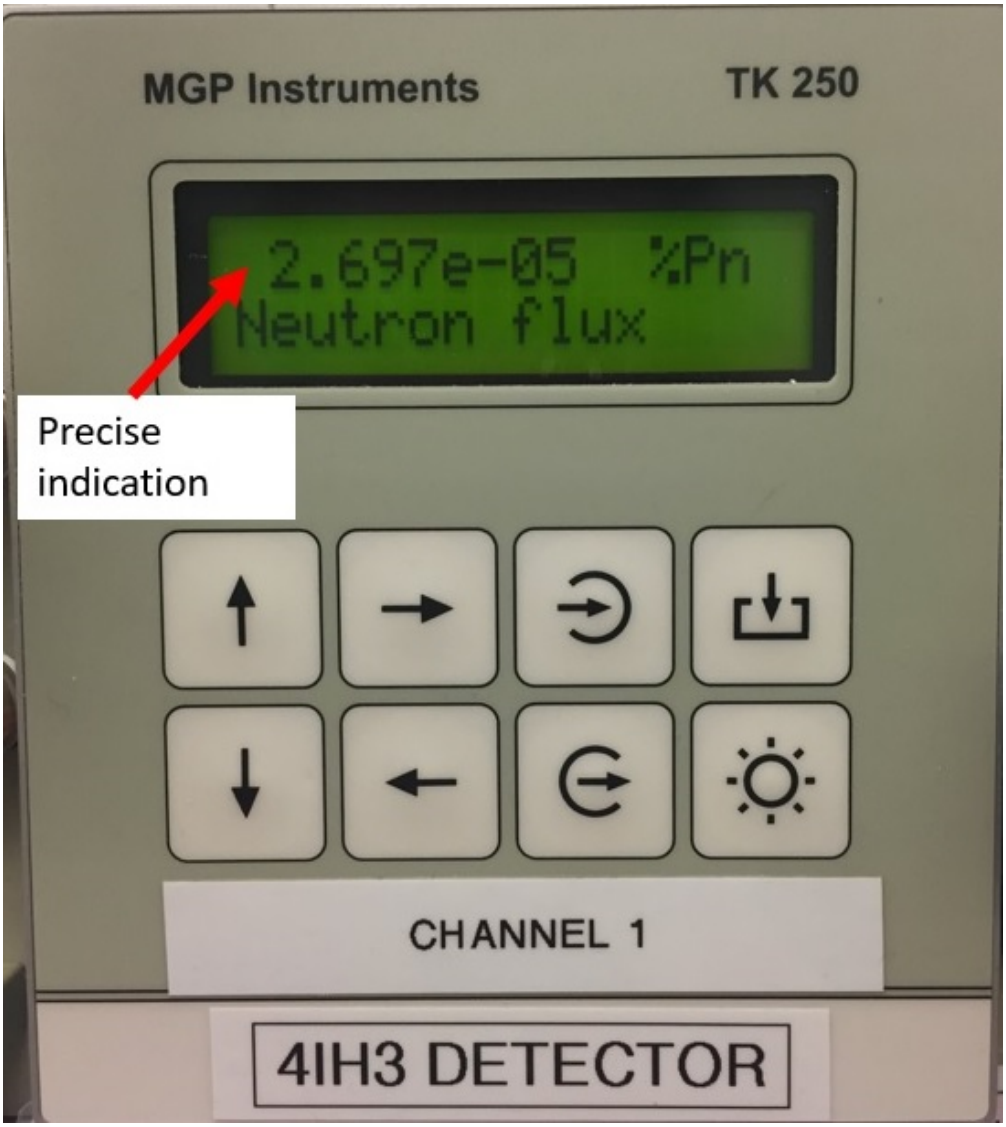

Figure 3.3: The digital display of the neutron flux located on each of the four DWK installations. The scram points are set with a precise digital value.

The display located on each of the four DWK installations is used to set the scram setpoints for each of the DWK channels. In order to set the scrams, a series of buttons must be pressed. The digital display provides a thousandth decimal point accurate indication of reactor neutron flux.

3.2 Thermal Power Calculation

In order to determine the accuracy of the four DWK channels, they were compared to thermal reactor power. Thermal reactor power

$$P = 2.62 \times 10^{-4} \times F_P \times \Delta T_P \tag{3.1}$$

$$R = 2.91 \times 10^{-4} \times F_R \times \Delta T_R \tag{3.2}$$

$$S = 2.62 \times 10^{-4} \times F_S \times \Delta T_S \tag{3.3}$$

$$TP = P + R + S, \tag{3.4}$$

where P, R, and S correspond to the calculations for the primary, reflector, and shield systems respectively, F_i corresponds to the respective system flow [gpm], and ΔT_i corresponds to the difference between the outlet and inlet temperatures [$^\circ C$] for each respective system [11]. The constants in each of the P, R, and S equations were determined through the specific heat of vaporization of H_2O for the primary and shield systems and D_2O for the reflector system. Summing the primary, reflector, and shield parts yields TP, the thermal reactor power. Equation 3.4 was used to determine thermal power [11].

3.3 Convert DWK Detected Neutron Flux to Measured Reactor Power

In order to determine what the DWK reactor power was for each of the newly installed DWK channels, the signal for neutron flux detected by each channel had to undergo a conversion. The same equation was used to convert the detected signal to reactor power for each of the DWK's. The equation for this conversion is

$$DP = 5.9 \times 10^{a+(b/v)}, \tag{3.5}$$

where DP is the DWK reactor power, a and b are constants, with $a = -8.0025$ and $b = 0.000253343$, and v is the DWK detected signal [12]. The flux to reactor power conversion was performed on each of the four DWK detected signals. Signals were recorded each minute for the duration of recording time.

3.4 Uncertainties of Thermal Power vs. DWK Power Measurements

The thermal power is calculated through the combination of several values, each of which has a specific uncertainty associated with it. Thus, when combining the system flow rates and temperatures, the uncertainties have to be compounded as well. When multiplying by a measurement that has an uncertainty by a constant, the uncertainty is not affected [13].

When adding multiple measurements with associated uncertainties, each measurement's uncertainties are added in quadrature [13]. An example of how the final uncertainty can be determined when combining in quadrature is,

$$\sigma_F = \sqrt{\sigma_P^2 + \sigma_R^2 + \sigma_S^2}, \tag{3.6}$$

where σ_F is the final uncertainty of the combination and $\sigma_{P,R,S}$ correspond to the uncertainties of the primary, reflective, and shield systems respectively [13].

When multiplying by a constant, the uncertainty is also multiplied by that constant [13]. An example of how the final uncertainty can be reached when combining in quadrature is,

$$\sigma_F = C_i * \sigma_i, \tag{3.7}$$

where σ_F is the final uncertainty of the combination, C_i is a constant, and σ_i, where $i = P, R, S$ for the primary, reflective, and shield, corresponds to the uncertainties of each respective system [13].

When multiplying multiple measurements with associated uncertainties, each measurement's uncertainties are summed [13]. An example of how the final uncertainty can be reached when combining measurements, each with their own uncertainty is,

$$\sigma_F = \sigma_P + \sigma_R + \sigma_S, \tag{3.8}$$

where σ_F is the final uncertainty of the combination and $\sigma_{P,R,S}$ corresponds to the uncertainties of the primary, reflective, and shield systems respectively [13].

Ultimately, the combination of many systems and indications contributes to a larger uncertainty and thus a larger spread of the calculated thermal power especially when compared to the spread of the DWK power measurements. The DWK reactor power measurements only have the uncertainty associated with the detector. This suggests that their readings are more precise than thermal power.

3.5 Recorded Reactor Power Data

In order to determine the accuracy of each of the DWK channels, the current detected by each of their fission chambers was recorded (and converted to reactor power using Equation 3.5) every minute over two separate reactor operating periods. The thermal power of the reactor was also calculated using Equation 3.4 every minute over the same operating periods to compare with the reactor power measured by each of the DWK's. The first operating period was from 05-5-17 to 05-22-17. The DWK 1-4 Measured Reactor Power and Thermal Reactor Power calculated over the 17 days is shown in Figure 3.4.

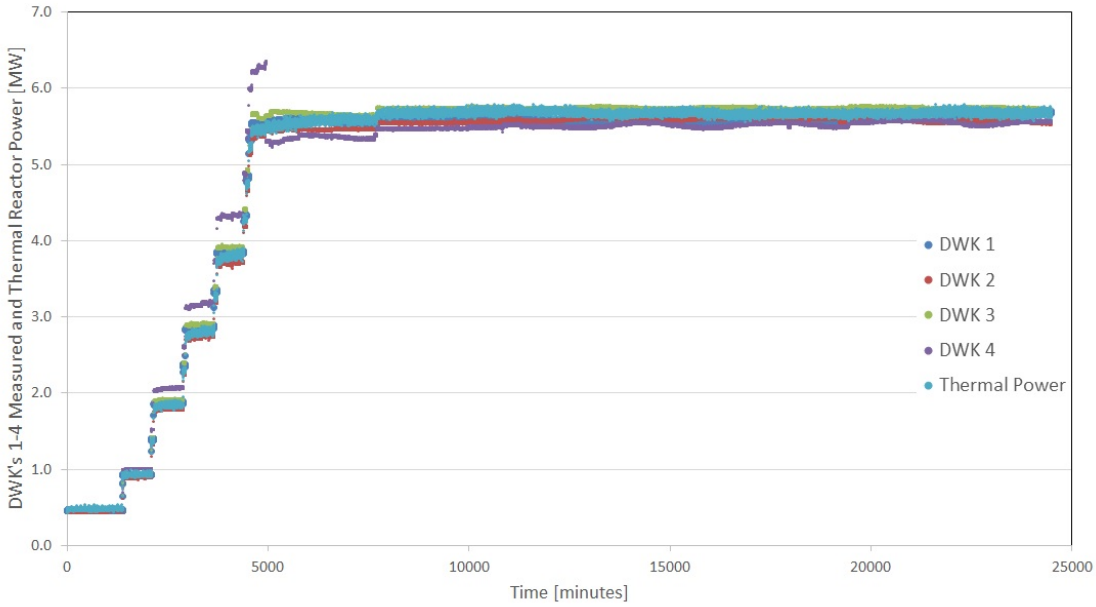

Figure 3.4: Reactor power measured by DWK's 1-4 and thermal reactor power calculated from 05-05-17 to 05-22-17. Reactor power measurements were taken every minute from shutdown reactor power (0 MW) to full operation reactor power (5.7 MW) over approximately 17 days. The variation between the thermal reactor power and the DWK measured reactor power measured by each of the 4 DWK channels can be seen.

Figure 3.4 shows the power detected by the DWK's and the calculated thermal reactor power from a reactor startup to approximately 5.7 MW on 05-05-17 until 05-22-17. Reactor power begins at 0 MW and increases in steps of 0.5 MW until reactor thermal power reaches approximately 5.7 MW. The steps of power increases can be seen in Figure 3.4.

A second set of power recordings was taken between 10-13-17 and 12-19-17 over a full reactor operating period. The reactor power measured by the four DWK channels and thermal power calculations were recorded every minute over approximately 67 days. The reactor power measured by the four DWK channels and thermal reactor power are shown over time in Figure 3.5.

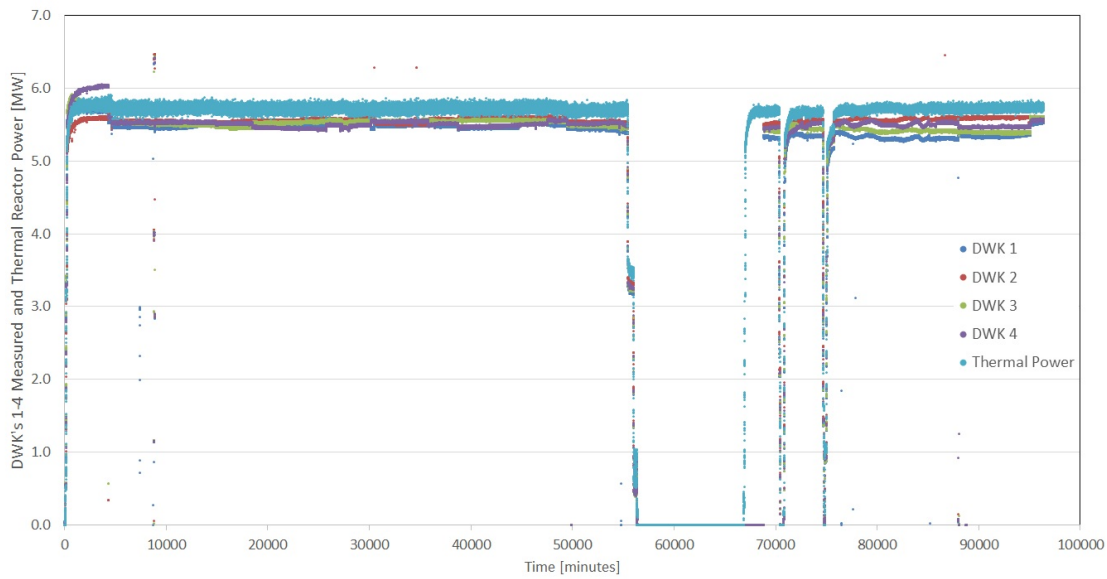

Figure 3.5: Reactor power measured by DWK's 1-4 compared to thermal reactor power. Reactor power measurements were taken every minute from shutdown reactor power (0 MW) to full operation reactor power (5.7 MW) over an entire operating period and fuel cycle of the reactor (approximately 67 days. The variation between the thermal reactor power and the DWK measured reactor power measured by each of the 4 DWK channels can be seen.

The long nearly vertical scatter points indicate the power detected by the four DWK's and thermal reactor power shown in Figure 3.5 during startup or shutdown situations over the operating period. Steady-state operation occurs primarily between 10000 and 50000 minutes. Thermal reactor power seems to be higher than the DWK reactor power measurements for all of the channels.

3.6 Statistical Analysis of Power Measurements

In order to determine how precise sample data sets are, the mean and standard deviation of a sample set can be calculated. [14]. The mean or average reactor power for each of the DWK channels and the reactor thermal power was calculated from the data taken during steady-state operation. The mean was determined by averaging each of the power measurements from 8500 to 17500 minutes for the 05-05-17 to 05-22-17 data set. The mean can be calculated by

$$\bar{x} = \frac{\sum x_i}{n}, \tag{3.9}$$

where $\bar{x}$ represents the mean, $\sum x_i$ represents the summation of each of the power measurements, and n represents the number of reactor power measurements [14].

The standard deviation, which indicates a value that when added and subtracted to the mean creates an interval in which 66% of the data set will fall. The equation to calculate the standard deviation for each DWK and the thermal reactor power is

$$\sigma = \sqrt{\frac{\sum(x_i - \bar{x})^2}{n-1}}, \tag{3.10}$$

where $\bar{x}$ represents the mean, x_i indicates the power measurement, and n indicates the number of reactor power measurements [14]. The standard deviation can provide an interval in which 66% of any measurements taken at the steady-state operation level will fall within that interval. The minimum of that interval will be equal to $\bar{x} - 3\sigma$ and the maximum of that interval will be equal to $\bar{x} + 3\sigma$. The standard deviation can be further compounded to yield an interval that corresponds to a 99.7% confidence that any measurement taken at the steady state operation will fall within that interval. This is referred to as the 3σ value. The minimum of the 99.7% confidence (or 3σ) interval is

$$minimum = \bar{x} - 3\sigma, \tag{3.11}$$

where $\bar{x}$ represents the mean. The maximum of the 99.7% confidence (or 3σ) interval is

$$maximum = \bar{x} + 3\sigma \tag{3.12}$$

Percent discrepancy can be a useful determination for comparing how accurate a measurement is. The average percent discrepancy between a set of experimental values and the corresponding accepted values can be determined with

$$\epsilon = \frac{\sum_{i=1}^{n} \frac{A_i - E_i}{A_i}}{n} \tag{3.13}$$

where ϵ is the average percent discrepancy, n is the number of reactor power measurements taken, A_i corresponds to each accepted value for reactor power, in this case each measurement of thermal power which is taken to be the actual reactor power, and E_i corresponds to each experimental value for reactor power, or the DWK detected power [14]. This can be used to determine an average percent discrepancy between the measurements made by the DWK channels and the thermal power recorded reactor power. Taking the thermal power to be the accepted value, and the reactor power measured by each of the DWK channels at that same minute over a steady-state operation period to be the experimental value, a percent discrepancy for each of the DWK channel's averages can be deduced.

3.6.1 Modelling of Drift

Modelling of the neutron flux at the 3GV and 4TH ports was performed using MCNP5/1.60 standard Monte Carlo code by Dr. Kaichao Sun of the MITR-II [15]. The goal of the modelling was to determine the change in neutron flux at the 3GV and 4TH ports as the shim bank height changed in the core [15]. 4TH ports were analyzed in place of 4IH ports because there was a lack of information regarding the exact axial and radial locations of the 4IH ports. The 4TH and 4IH ports are both located under the core tank, and thus should both show the same trends in the change of neutron flux [15].

Chapter 4

Results and Discussion

4.1 05-05-17 to 05-22-17 Statistics Quantification

The means, sample standard deviations, and three sigma values for each of the DWK channels and the thermal reactor power measurements from the steady-state operation from minute 8500 to 17500 of the 05-05-17 to 05-22-2017 data recordings were determined. Steady-state analysis was chosen to begin at 8500 minutes, or approximately 6 days, because 6 days after start-up, the reactor is in a state of xenon-equilibrium which indicates that there would be minimal movement of the shim blades which could change the signals detected by the DWK's. Also, after 6 days the reactor is in a state of thermal equilibrium, in which the fission power deposition in the primary, secondary, and shield systems should be constant, so the thermal power calculation should also be in steady-state equilibrium. The time frame 8500 to 17500 minutes is equivalent to approximately 6.25 days which provides an adequate amount for steady-state analysis. The results of this analysis are reported in Table 4.1.

	DWK 1	DWK 2	DWK 3	DWK 4	Thermal Power
Mean [MW]	5.586	5.582	5.741	5.503	5.679
Std. Dev. [MW]	0.01444	0.02371	0.01211	0.02451	0.02947
3σ [MW]	0.04334	0.07113	0.03633	0.07353	0.08842

Table 4.1: Means, standard deviations, and 3-sigma values for steady-state operation from 8500 to 17500 minutes of the 05-05-17 to 05-22-17 DWK's 1-4 and thermal reactor power recording. The mean indicates the average power detected by each of the channels and the thermally calculated power. The standard deviation indicates the range $\pm$ the mean in which 66% of the data exists for each of the channels and the thermal power. The 3-sigma value indicates the range $\pm$ the mean in which 99.7% of the data exists for each of the channels and the thermal power.

The means were calculated using Equation 3.9, the sample standard deviations were determined using Equation 3.10, and the 3σ value was determined by multiplying the standard deviation by 3. The σ values indicate that with 99.7% confidence, the power detected by a channel will fall within $\pm$ the three sigma value of the mean. Thus, looking at DWK 1,

whose mean is 5.586287, with 99.7% confidence, the steady-state neutron power measured by DWK 1 will be between $5.586287 - 0.043343 = 5.542945$ and $5.586287 + 0.043343 = 5.62963$. The minimum and maximum reactor powers, calculated using Equations 3.11 and 3.12 respectively, of the range of the calculated 99.7% confidence intervals for each of the DWK channels and thermal reactor power during steady state operation are shown in Table 4.1.

	DWK 1	DWK 2	DWK 3	DWK 4	Thermal Power
Minimum [MW]	5.542945	5.511699	5.705424	5.430074	5.590651
Maximum [MW]	5.62963	5.65397	5.778093	5.57714	5.76751
3σ Range Percent of Mean [%]	1.55	2.54	1.26	2.67	3.11

Table 4.2: 99% confidence reactor power ranges for DWK's 1-4 and thermal power. This indicates that at steady-state operation of approximately 5.67 MW thermal reactor power, the power measured by any of the DWK's 1-4 or the power calculated using the thermal power will fall between their respective minimum and maximum reactor power levels with a 99.7% probability. The range of each of the 99.7% confidence intervals was divided by the mean reactor power for each DWK and thermal power. Each DWK has a 3σ range that is less than 2.7% of their respective means. The thermal power 3σ range is 3.11% of its mean, meaning it has a greater uncertainty than the DWK detectors.

The ranges of the 99.7% confidence intervals for each of the channels and the thermal power do not entirely overlap. The minimum of DWK's 1, 2, and 4 are lower than the minimum of the thermal power. The maximum power of DWK 3 is greater than the maximum thermal reactor power calculated. This indicates that there is a miscalculation of reactor power being made by each of the DWK's and they require calibration in order to accurately indicate the thermal reactor power.

In order to determine how the change in power measured by the DWK channels compared to the change in thermal reactor power, the DWK's 1-4 detected reactor power over the 05-05-2017 startup (minutes 1 to 4953) were plotted against thermal reactor power. During this time period, the DWK required calibration. Prior to minute 5000, the DWK was recalibrated. No effect was seen on the linearity of the system. R^2 tests for a linear regression model were then completed on each of the DWK channels to determine the linearity of the power increases detected by each of the DWK's. The comparison DWK channel reactor power and thermal reactor power is shown in Figure 4.1.

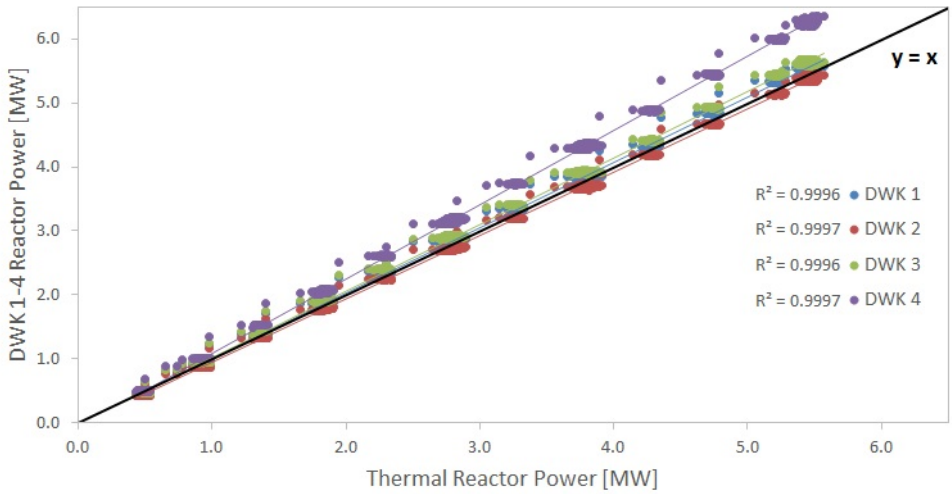

Figure 4.1: Reactor power measured by DWK's 1-4 during a startup on 05-05-2017 was plotted against the thermal power measured at the same time. R^2 tests for a linear regression model were then completed for each of the DWK channels to determine the linearity of the power increases detected by each channel. Each of the four channels was found to have an R^2 value that was greater than or equal to 0.9996, where $R^2 = 1$ indicates an exactly linear relationship between power increments. A $y = x$ line was included to show the variation in the slopes of each of the DWK channels when compared to thermal power. The slopes of the lines of each of the DWK channels when compared to thermal power appear to be different, likely due to their various locations around the core as seen in Figure 2.8.

The increase in reactor power detected by DWK's 1-4 was found to be nearly linear for each of the DWK channels. The R^2 values for a linear regression fit for each of the DWK channels was equal to 0.996 for DWK's 1 and 3 and equal to 0.997 for DWK's 2 and 4 . This indicates that the DWK's scale nearly linearly with increases in thermal reactor power. Therefore adjustments can easily be made to the setpoints of the DWK's such that they align with thermal reactor power. The four DWK channels were compared to $y = x$, which is a sample equation of a line that indicates a perfectly linear relationship between DWK reactor power and thermal reactor power. The

4.2 10-13-17 to 12-19-17 Statistics Quantification

The mean, standard deviations, and 3σ values were also calculated for the reactor power measured by DWK channels 1-4 and the thermal reactor power during steady-state operation between 10-13-17 and 12-19-17. The calculated means, standard deviations, and 3σ values for each of the channels and thermal power are shown in Table 4.3.

	DWK 1	DWK 2	DWK 3	DWK 4	Thermal Power
Mean [MW]	5.488	5.541	5.545	5.526	5.723
Std. Dev. [MW]	0.01281	0.01133	0.01425	0.01153	0.03932
3σ [MW]	0.03844	0.03401	0.04275	0.03461	0.11798

Table 4.3: Means, standard deviations, and 3σ values for steady-state operation of the 10-13-17 to 12-19-17 DWK's 1-4 and thermal reactor power recording. The mean indicates the average power detected by each of the channels and the thermally calculated power. The standard deviation indicates the range $\pm$ the mean in which 66% of the recorded power values exist for each channel and thermal power. The 3σ value indicates the range $\pm$ the mean in which 99.7% of the power values exist for each channel and thermal power.

The average thermal power was greater than all of the mean measured power for each of the DWK channels indicating that the DWK's were likely under calibrated. The minimums and maximums of the 3σ intervals for each of the DWK's and the thermal power were determined based upon the second data set from 10-13-17 to 12-19-17 and can be seen in Table 4.4.

	DWK 1	DWK 2	DWK 3	DWK 4	Thermal Power
Minimum Power [MW]	5.450	5.507	5.502	5.491	5.605
Maximum Power [MW]	5.527	5.575	5.588	5.560	5.841
3σ Percent of Mean [%]	1.40	1.22	1.54	1.25	4.12

Table 4.4: 99.7% confidence reactor power ranges for DWK's 1-4 and thermal tower. This indicates that at steady-state operation of approximately 5.67 MW thermal reactor power, the power measured by any of the DWK's 1-4 or the power calculated using the thermal power will fall between their respective minimum and maximum reactor power levels with a 99.7% likelihood. The range of each of the 99.7% confidence intervals was divided by the mean reactor power for each DWK's mean reactor power value. Each DWK has a 3σ range that is less than 2% of their respective means. The thermal power 3σ range is 4.12% of its mean, meaning it has a greater standard deviation than the DWK detectors.

In this instance, the minimum of the thermal reactor power is still greater than the maximums of any of the DWK channels, again suggesting that the DWK channels were under calibrated over the operating period. Further each of the DWK channels has a 3σ range that is $< 2\%$ of their respective means. The thermal power 3σ range is 4.12% of its mean, indicating that the DWK detectors are more precise. This suggests that there is a greater uncertainty in the thermal power calculation which can be attributed to the summation of the uncertainties of the flow and temperature indications that are used to calculate thermal power as shown in Equation 3.4.

4.3 Fitted Normal Distributions

To further analyze the accuracy of the detector data, the reactor power values detected by the DWK's at steady-state operation (10000 to 30000 minutes, approximately 13.8 days) were grouped into power intervals (known as bins) and plotted as histograms to see how the steady-state data for each DWK was distributed. Further, the mean and standard deviation were used to create a fitted normal distribution of the data set for each DWK and thermal power. A normal distribution shows the spread of the data, it provides the location of the mean or average value as well as the 99.7% range of power indications. Normal distributions were created for each of the four DWK channels and the thermal reactor power using their respective means and standard deviations. These distributions were then plotted over the actual histogram data in order to determine how well the data fit to a normal distribution. The normal distribution plotted over the steady-state equilibrium data of DWK 1 is shown in Figure 4.2.

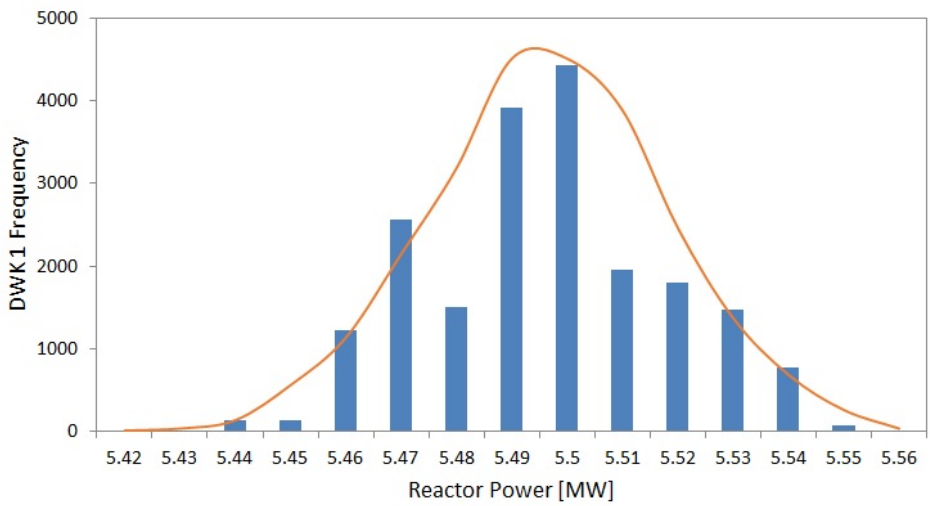

Figure 4.2: The steady-state power detected by DWK 1 from minute 10000 to 30000 during the 10-13-17 to 12-19-17 operation period was grouped into energy power intervals of 0.01 MW from 5.42 MW to 5.56 MW (which correspond to the minimum and maximum 3σ values for DWK 1). Then a fitted normal distribution (depicted by the orange line) was plotted over the actual energy data using the mean and standard deviation of DWK 1. The normal distribution plotted shows the range of 99.7% of the DWK 1 power measurements.

The DWK 1 steady-state operation data seems to fit a normal distribution. A normal distribution is shaped like a bell curve. The histogram power data from DWK 1 shows a peak in the center (indicative of the average) with the frequency of power measurements decreasing as the reactor power moved away from the average. This pattern matches that of a normal distribution. This indicates that approximately 68% of the data falls within one standard deviation of the mean and that approximately 99.7% of the data falls within 3σ of the mean. Therefore, the use of a linear regression to model the DWK 1 data is appropriate and it is verified or correct to assume that 99.7% of the detected reactor power is within

3σ of its mean. The same time interval of data was plotted as a histogram for the thermal power overlaid by a fitted normal distribution using the mean and standard deviation for thermal power. This plot is shown below in Figure 4.3.

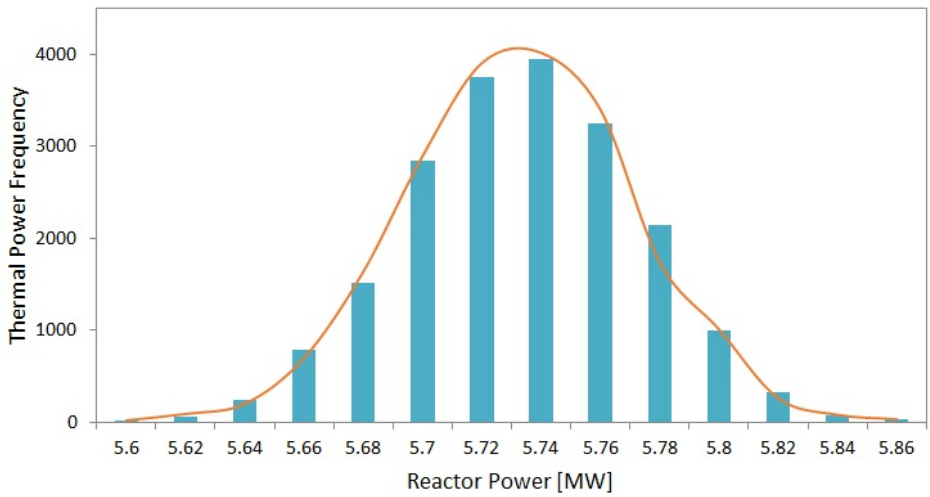

Figure 4.3: The steady-state thermal power from minute 10000 to 30000 during the 10-13-17 to 12-19-17 operation period was grouped into energy power intervals of 0.02 MW from 5.6 MW to 5.86 MW (which correspond to the minimum and maximum 3σ values for thermal power over this range). Then a fitted normal distribution (depicted by the orange line) was plotted over the actual energy data using the mean and standard deviation of thermal power. The normal distribution plotted shows the range of 99.7% of the thermal power power measurements.

The thermal power steady-state operation data clearly fits a normal distribution. The histogram thermal power shows a distinct peak located in the center (indicative of the average) with the frequency of power measurements decreasing steadily as the thermal power moved away from the center or average. This pattern matches exactly that of a normal distribution. This indicates that approximately 68% of the data falls within one standard deviation of the mean and that approximately 99.7% of the data falls within 3σ of the mean. Therefore, the use of a linear regression to model the thermal power data is appropriate and it is verified or correct to assume that 99.7% of the thermal reactor power is within 3σ of its mean. The same histogram and normal fitted distribution analysis was performed for each of the DWK channels and can be found in the appendix.

In order to indicate the relationship between the measured reactor power by the DWK channels and thermal power, each set of data was fitted to a normal distribution using each channel and thermal power's respective means and standard deviations. The fitted normal distributions for thermal power and DWK 1 were plotted on the same axis in Figure 4.4.

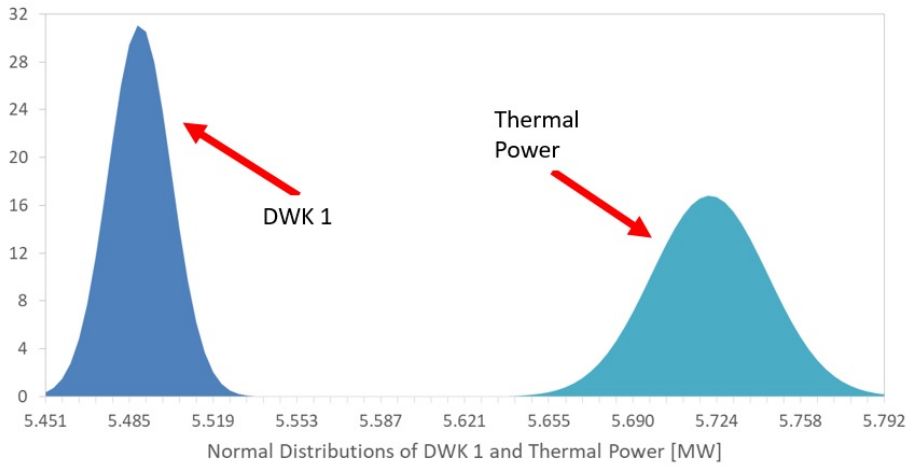

Figure 4.4: The fitted normal distributions for DWK 1 and thermal power were plotted using their means and standard deviations. The fitted normal distributions show the range of 99.7% of the DWK 1 and thermal power measurements respectively. The two fitted normal distributions do not intersect indicating there is likely an offset between the DWK channel calibration and actual thermal power. The spread of the thermal power is greater than that of the DWK indicating that the DWK detector is likely more precise.

The fitted normal distributions for DWK 1 and thermal power do not intersect. The larger spread of the thermal power is a result of the greater uncertainty in its calculation which combines multiple system flows and temperatures. However, the uncertainty is not large enough to account for the 4% difference between the two average reactor power. Therefore, it is likely that there exists a coefficient offset or calibration error between DWK 1 and thermal power. Because the relationship between the two is linear, it is possible in future work to determine this coefficient or new calibration equation. Due to the narrow spread of DWK 1, it is likely that if it can be adjusted to provide a more accurate representation of the thermal power, it will be very precise in its reactor power indications.

4.4 Average Percent Discrepancy

To get a quantitative value for the average percent discrepancy between each of the four DWK's measurements and the average thermal reactor power, Equation 3.13 was applied to steady-state operation at approximately 5.7 MW for both the 05-05-17 to 05-22-17 and 10-13-17 to 12-19-17 data. The average percent discrepancy for each of the DWK channels when compared to the thermal reactor power over both operating periods is shown in Table 4.5.

	DWK 1	DWK 2	DWK 3	DWK 4
Average % Discrepancy 05-05-17 [%]	1.6	1.7	-1.1	3.1
Average % Discrepancy 10-13-17 [%]	4.0	3.0	3.7	4.09

Table 4.5: The average percent discrepancies between each of the DWK channel measurements and the actual thermal reactor power during steady state operation of about 5.7 MW from 8500 to 13500 minutes from the 05-05-17 to 05-22-17 data (approximately 6.25 days) and from 10000 to 30000 minutes from the 10-13-17 to 12-19-17 data (approximately 13.8 days). For the 05-05-17 cycle, the average percent discrepancies were around 2% for DWK's 1, 2, and 3. DWK 4 had a percent discrepancy of 3.1%. For the 10-13-17 cycle, the average percent discrepancies were approximately 4% for DWK's 1, 3, and 4 and 3% for DWK 2.

The average percent discrepancy was determined from the discrepancy between the DWK channel measurements and the actual thermal reactor power during steady state operation of about 5.7 MW from 8500 to 13500 minutes from the 05-05-17 to 05-22-17 data (approximately 6.25 days) and from 10000 to 30000 minutes from the 10-13-17 to 12-19-17 data (approximately 13.8 days). At this time, the reactor would have been at xenon equilibrium and the reactor power was at its steady state operation of approximately 5.7 MW thermal. Each of the DWK detectors was found to have an average percent discrepancy of less than 4.1%. 4.1% corresponds to the average percent discrepancy that was determined by modelling of the new DWK detectors. The average percent discrepancy is different for each channel. This could be a result of their varying location around the reactor core. It also suggests that the reactor power is equal across the core, and there is minimal power peaking.

In order to see if the linearity of the DWK's and thermal power held over a full reactor operating period, the DWK power level measured each minute was plotted against the thermal power calculated each minute during the 10-13-2017 to 12-19-2017 operating period.

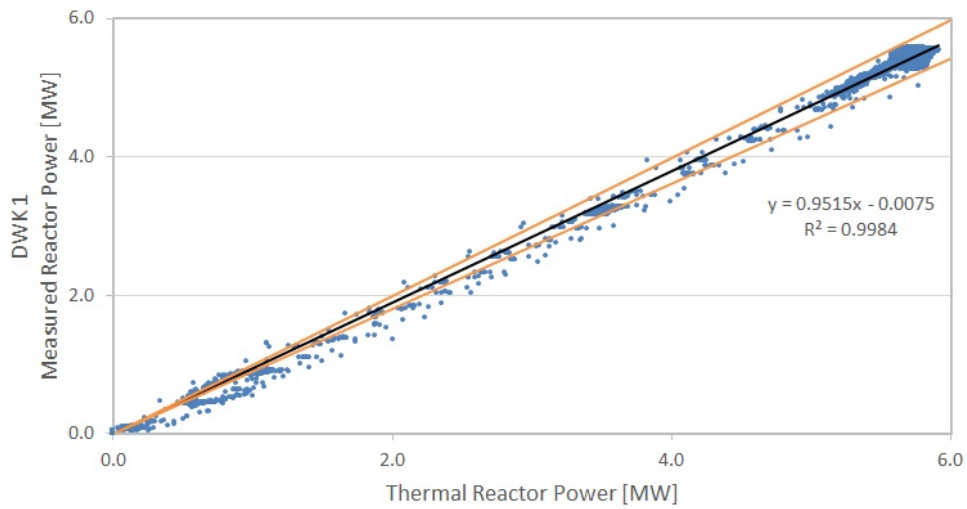

Figure 4.5: Reactor power measured by DWK 1 from 10-13-2017 to 12-19-2017 was plotted against the thermal power measured at the same time. R^2 tests for a linear regression model were then completed for each of the DWK channels to determine the linearity of their relationship to thermal reactor power. DWK 1 was found to have $R^2 = 0.9984$. discrepancy lines at $\pm 5\%$ were included that show at steady-state operation, the majority of the data was within $\pm 5\%$ of the average.

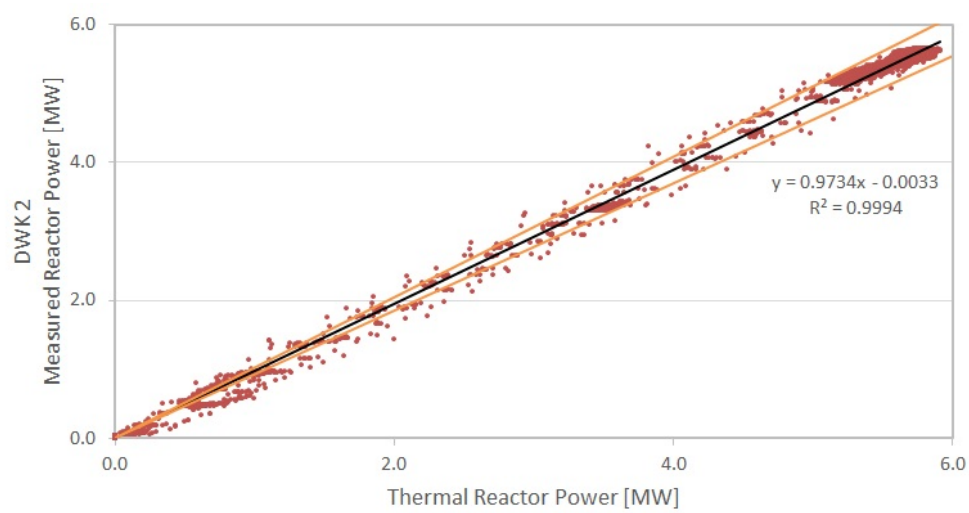

Figure 4.6: Reactor power measured by DWK 2 from 10-13-2017 to 12-19-2017 was plotted against the thermal power measured at the same time. R^2 tests for a linear regression model were then completed for each of the DWK channels to determine the linearity of their relationship to thermal reactor power. DWK 2 was found to have $R^2 = 0.9984$. discrepancy lines at $\pm 5\%$ were included that show at steady-state operation, the majority of the data was within $\pm 5\%$ of the average.

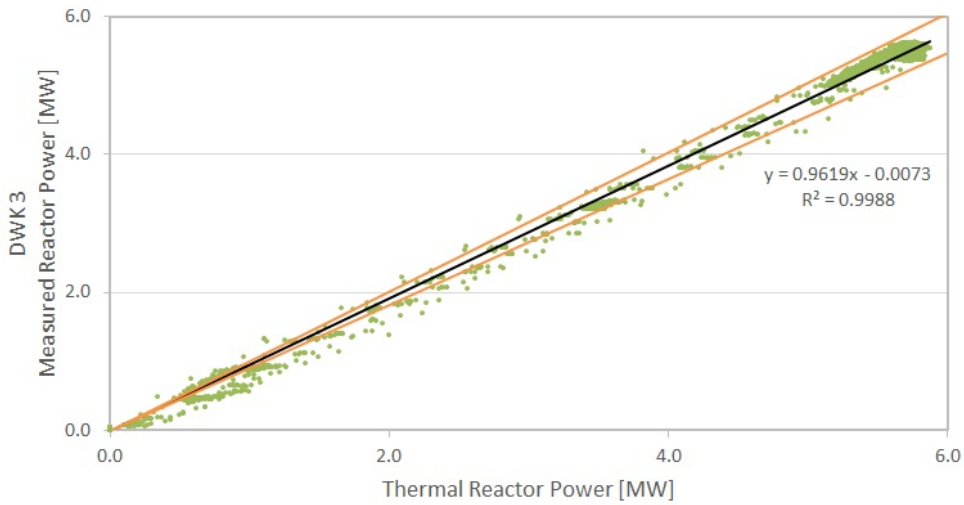

Figure 4.7: Reactor power measured by DWK 3 from 10-13-2017 to 12-19-2017 was plotted against the thermal power measured at the same time. R^2 tests for a linear regression model were then completed for each of the DWK channels to determine the linearity of their relationship to thermal reactor power. DWK 3 was found to have $R^2 = 0.9988$. discrepancy lines at $\pm 5\%$ were included that show at steady-state operation, the majority of the data was within $\pm 5\%$ of the average.

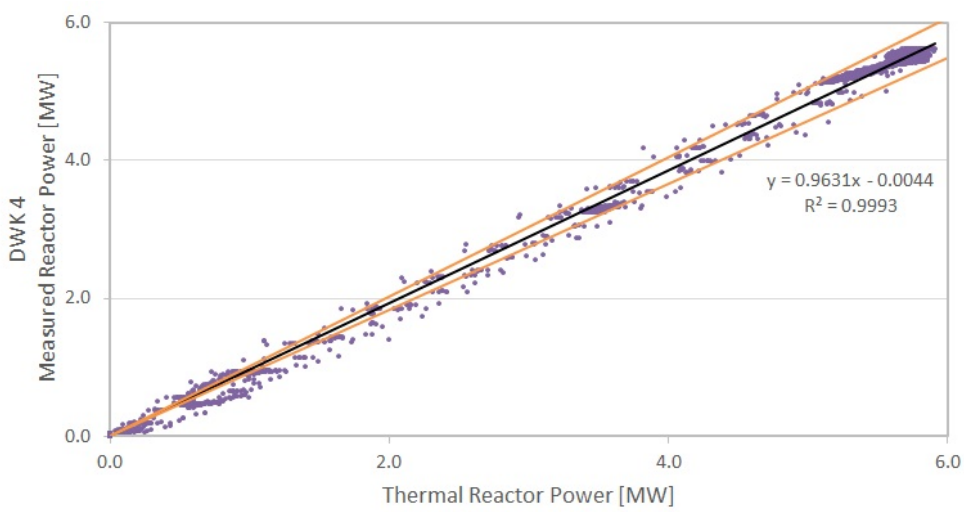

Figure 4.8: Reactor power measured by DWK 4 from 10-13-2017 to 12-19-2017 was plotted against the thermal power measured at the same time. R^2 tests for a linear regression model were then completed for each of the DWK channels to determine the linearity of their relationship to thermal reactor power. DWK 4 was found to have $R^2 = 0.9993$. discrepancy lines at $\pm 5\%$ were included that show at steady-state operation, the majority of the data was within $\pm 5\%$ of the average.

Each of the four DWK channels has a nearly perfect linearity relationship (perfectly

linear, $R^2 = 1$) with thermal reactor power over the 10-13-2017 to 12-19-2017 operating period. ±5% discrepancy bars were included on Figures 4.5, 4.6, 4.7, and 4.8 that indicate at steady-state operation, the majority of the data falls within ±5% of the average. This validates the average percent discrepancy calculated using Equation 3.13. At low power levels, the data does not fall within these discrepancy bars. This is likely because the DWK detected power (neutron flux based) reacts faster than the thermal power to increases in temperature.

This indicates that the DWK channels do not drift immensely over a full operating period on average. In order to quantify the amount by which they do drift due to shim bank height change, it is necessary to compare the relationship between thermal reactor power and DWK measured power for each of the channels at the beginning of the operating period and at the end of the operating period.

4.5 Quantifying DWK Drift

In order to determine if there was any drift in the signals detected by the DWK channels over an operating period, DWK measurements were recorded every ten minutes at steady-state operation from 09-09-17 to 09-25-17 (approximately 16 days) and 10-16-17 to 11-13-17 (approximately 28 days) for each of the four channels. These measurements were converted to reactor power and the percent discrepancy between each of the DWK's measurements and the calculated thermal power was determined for each data point. The percent discrepancy between DWK 1 and thermal power measurements at steady-state operation from 09-09-17 to 09-25-17 is shown in Figure 4.9.

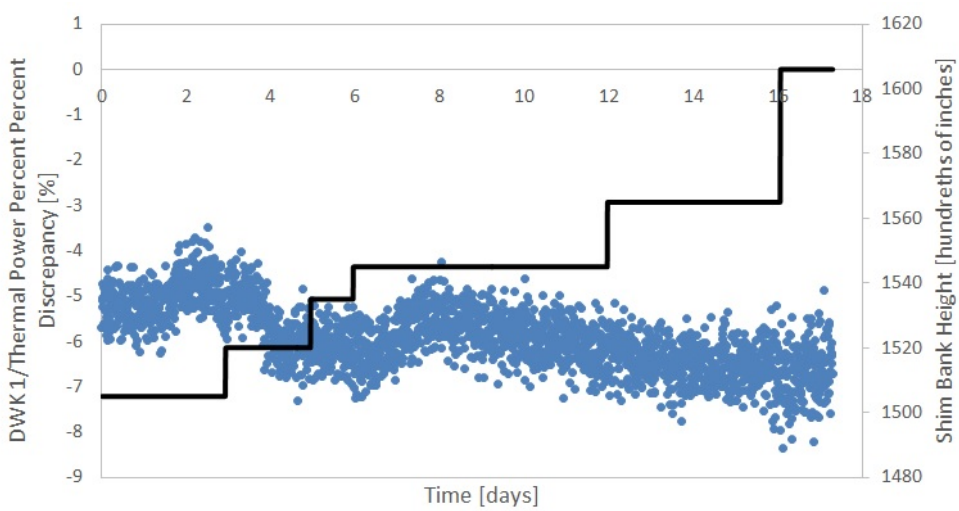

Figure 4.9: The percent discrepancy between DWK 1 and thermal power during steady-state operation is plotted every ten minutes over 16 days from 09-09-17 to 09-25-17. This plot is overlaid with a black line representing the shim bank height over the same time frame. The percent discrepancy seems to drift downwards from day 8 to day 16.

The same analysis was performed on DWK channels 2, 3, and 4; these plots can be

found in the appendix. The shim bank height increased 1.01 inches, from 15.05 to 16.06 inches, over the 16 days that were analyzed. From day 8 to day 16, there seems to be a slight increase in the percent discrepancys for all four of the DWK channels. In order to better compare the change in percent discrepancy as the operating period progressed, the percent discrepancy between the DWK channels and thermal power was averaged for each DWk channel individually at each shim bank height. The shim bank height was then plotted against both the average percent discrepancy for each DWK channel and the time in Figure 4.10.

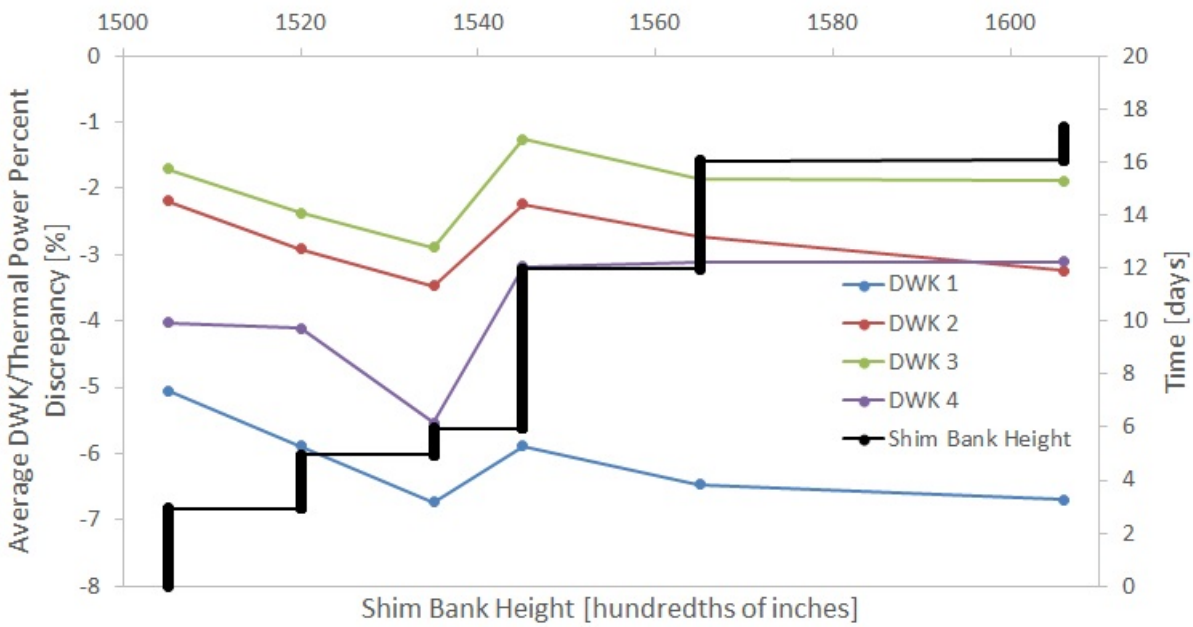

Figure 4.10: The average percent discrepancy between each DWK and thermal power during steady-state operation was plotted at each shim bank height position over 16 days from 09-09-17 to 09-25-17. This plot is overlaid with a black line representing the shim bank height over the same time frame. There seems to be no trend in the change of average percent discrepancy over the operating period, as shim bank height increased.

The percent discrepancy between DWK 1 and thermal power measurements at steady-state operation from 10-16-17 to 11-13-17 is shown in Figure 4.11.

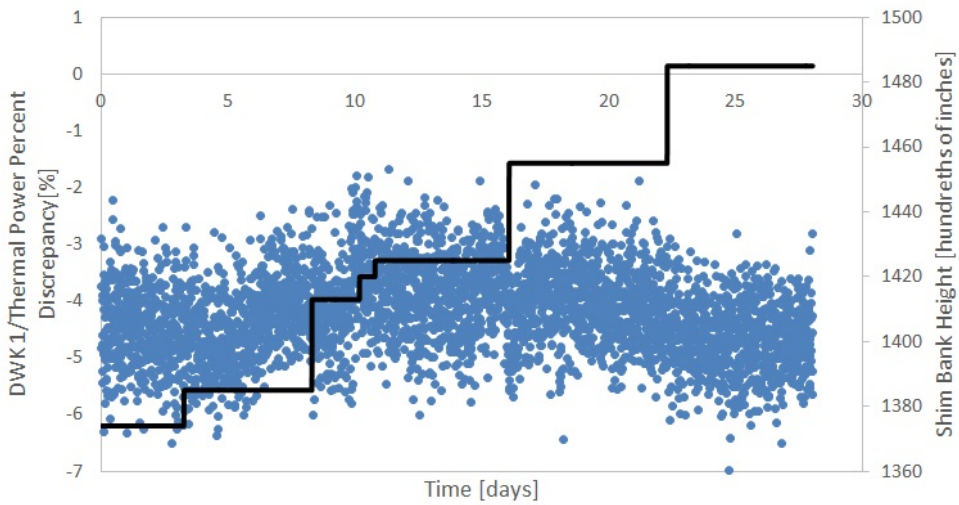

Figure 4.11: The percent discrepancy between DWK 1 and thermal power during steady-state operation is plotted every ten minutes over 28 days from 10-16-17 to 11-13-17. This plot is overlaid with a black line representing the shim bank height over the same time frame. The percent discrepancy seems to drift downwards from day 15 to day 28.

The same analysis was performed on DWK channels 2, 3, and 4; these plots can be found in the appendix. None of the four channels experienced significant drift over the four weeks that were analyzed. In the four weeks, the shim bank height increased from 13.74 inches to 14.85 inches, constituting a 1.11 inch total increase in shim bank height. The percent discrepancy did increase from day 15 until the end of the cycle for all DWK channels. When the shim bank height was held steady for over three days, the percent discrepancy between each DWK channel and the thermal power seemed to increase. Upon frequent increase in the bank height between days 9 and 11, the percent discrepancy deviated significantly for channels 1, 2, and 4 especially.

The reductions in percent discrepancy between the DWK channels and thermal power seem to occur after increases in the shim bank height after operating at the same bank height for multiple days. This could be due to the slower response of the thermal power indication than the DWK detectors. The DWK detectors measure a current from the neutron flux which changes more quickly than the response of system temperatures and flows when bank height is increased. Because the DWK's consistently under-predicted reactor power, when the signal they measure increases immediately following a shim bank height increase, their percent discrepancy compared to thermal power becomes smaller before the flow systems that are used to calculate thermal power reach equilibrium again. This results in a percent discrepancy reduction after changing the bank height.

In order to better compare the change in percent discrepancy as the operating period progressed, the percent discrepancy between the DWK channels and thermal power was averaged for each DWk channel individually at each shim bank height. The shim bank height was then plotted against both the average percent discrepancy for each DWK channel and the time in Figure 4.12.

Figure 4.12: The average percent discrepancy between each DWK and thermal power during steady-state operation was plotted at each shim bank height position over 28 days from 10-16-17 to 11-13-17. This plot is overlaid with a black line representing the shim bank height over the same time frame. There seems to be no trend in the change of average percent discrepancy over the operating period, as shim bank height increased.

The average percent discrepancy for DWK's 2 and 3 decreased over the 1.11 inch shim bank height increase during the operating period. The average percent discrepancy for DWK's 1 and 4 increased over the same shim bank height increase. Longer time frames of uninterrupted operation with no detector re-calibration would result in improved shim bank movement drift analysis of the DWK channels.

4.5.1 Modelling of Drift

At the start of the cycle, the shim bank was located at 9.3 inches and located at 16.9 inches at the end of the cycle [15]. The relative difference between the neutron flux measured by the DWK's at the start and end of the cycle in the 3GV ports was 6-8% above the core region and between -3% and 6% under the core region [15]. DWK's 2 and 4 are located in the 3GV ports which are vertical ports that are both above and below the core region. Thus, when the shim bank is raised over a cycle, DWK's 2 and 4 might experience a shift from a positive to a negative percent discrepancy when compared to the thermal power.

The relative difference between the neutron flux measured by the DWK's at the start and end of the modelled cycle in the 4TH ports was 5-7% [15]. This corresponds to the relative difference of the 3GV ports. DWK's 1 and 3 are located in the 4IH ports which are assumed to share qualities similar to the 4TH ports. In the below core region, where 4TH are located, the beginning neutron flux is higher than the ending neutron flux [15]. This would suggest that the neutron flux seen by DWK's 1 and 3 should be greater at the start

of the operating cycle (with a lower shim bank height) and decrease throughout the cycle (as shim bank height increased).

Although there is not enough experimentally gathered data to compare to the modelled data over an entire range of the shim bank height, the percent discrepancy of each of the DWK's does not trend up or down over only a 1 inch change in shim bank height. Thus, it is feasible that the modelled change in neutron flux over the full range of the shim bank height is as small as 6-8% for each of the four DWK's.

Chapter 5

Conclusion

5.1 Statistical Measurement Uncertainties

The average percent discrepancy between the newly installed DWK channels and the calculated thermal power is approximately 4% for each channel at steady-state operation. This corresponds to modelling that was performed on the DWK channels and their relation to the calculated thermal power. Each of the four DWK channels show that they detect reactor power according to a normal distribution. Thus, it is appropriate to say that 99.7% of the reactor power values detected by each DWK channel will be within 3σ of the mean, where each 3σ value was less than 1.6% of the mean for each DWK.

5.2 Calibration of DWK's

The current equation that is used to convert each DWK signal to reactor power should be modified. There is an exponential offset that is included in the equation which results in an average percent discrepancy between the DWK channels and thermal power of approximately 4%. With the removal of this offset in the conversion equation, the average percent discrepancy is approximately 2%. It is likely that there was an discrepancy in the original signal to reactor power conversion equation. This is due to the differing locations of the detectors around the core region; they each will have a different neutron flux based on their location. To get the most accurate reactor power indication possible, calibrating each of the DWK's individually with reactor power is crucial.

5.3 DWK Adjustment Over an Operating Cycle

The adjustment of the DWK's over a full operating cycle should be minimal due to the low 6-8% change in neutron flux detected by any of the DWK's when modelling steady-state operation at low and high shim bank heights. The experimental data analyzed over a shim bank height change of approximately 1" shows minimal variation in the percent discrepancy between DWK power and thermal power suggesting that there is minimal drift of the DWK neutron flux at steady-state operation over an entire fuel cycle.

Chapter 6

Suggestions for Future Work

Currently, the equation used to convert the signals detected by each of the DWK's to reactor power, Equation 3.5, is the same for each of the DWK's. Because the detectors are located in different locations surrounding the core, they will see varying levels of neutron flux and therefore each have a different relationship between what signal they detect and actual thermal power. Thus, it is recommended that new signal-to-reactor-power conversion equations are created for each DWK individually to get the most accurate reactor power indication possible.

For further verification of the accuracy and statistical analysis of the DWK channels at lower, non-steady-state operation, I would recommend that the reactor power be raised in 0.5 MW increments and permitted to stay at each of those power levels for at least an hour in order to collect a sufficient sample size of reactor power data for similar data analysis to be performed. This would improve the knowledge of average percent discrepancy and provide indication of each DWK channels' accuracy at lower power levels.

In order to accurately represent the percent discrepancy between the DWK channels' signals and thermal power, the conversion equation should be reassessed for its accuracy. This would likely result in a reduction in the calculated average percent discrepancy values for each of the DWK channels' at steady-state operation.

Finally in order to verify completely the modelling performed on 3GV and 4TH neutron flux at low and high shim bank heights, DWK data should be taken over a full operating period at constant operation. This would provide the best possible indication of DWK drift, if any, existed at varying shim bank heights. From this, the need for adjustment of the DWK calibration during a fuel cycle could be determined.

Chapter 7

Appendix

DWK channels 2, 3, and 4 steady-state reactor powers from minute 10000 to 30000 (approximately 13.8 days) during the 10-13-17 to 12-19-17 operating period were plotted as histograms with varying energy bin sizes and bounds. Normal distributions were then developed using random number generation and the means and standard deviations of each channel respectively. The normal distribution was then overlaid onto the histogram plot to provide an indication of how well the given data fits a normal distribution. These are shown in Figures 7.1, 7.2, and 7.3 below.

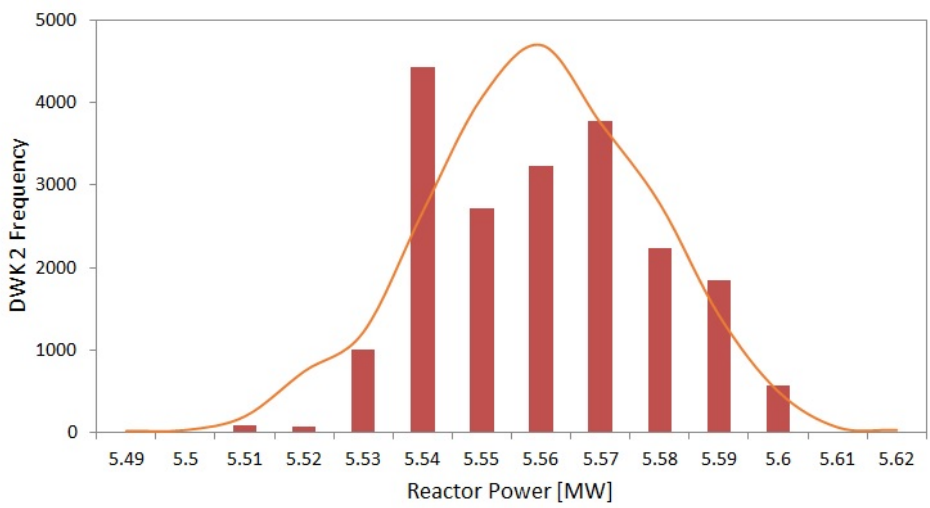

Figure 7.1: The steady-state power detected by DWK 2 from minute 10000 to 30000 during the 10-13-17 to 12-19-17 operation period was grouped into energy power intervals of 0.01 MW from 5.49 MW to 5.62 MW (which correspond to the minimum and maximum 3σ values for DWK 2). Then a fitted normal distribution (depicted by the orange line) was plotted over the actual energy data using the mean and standard deviation of DWK 2. The normal distribution plotted shows the range of 99.7% of the DWK 2 power measurements.

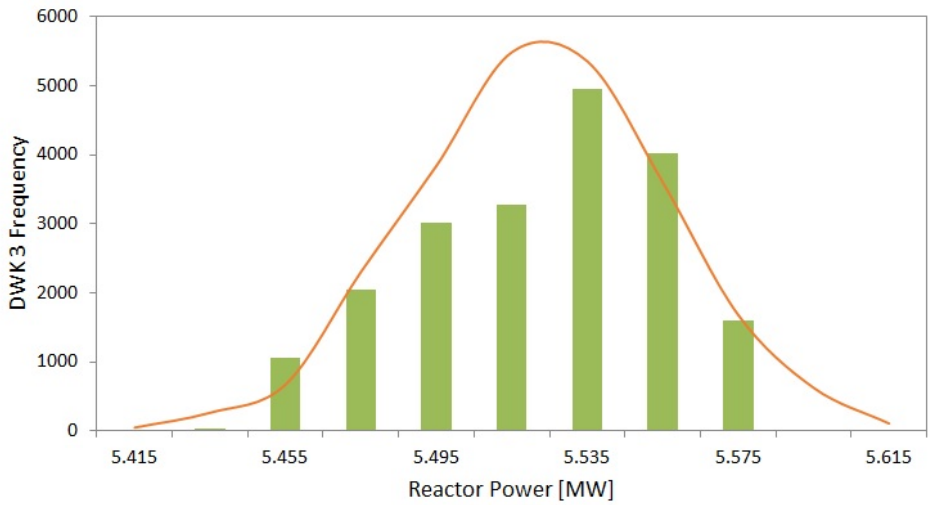

Figure 7.2: The steady-state power detected by DWK 3 from minute 10000 to 30000 during the 10-13-17 to 12-19-17 operation period was grouped into energy power intervals of 0.02 MW from 5.415 MW to 5.615 MW (which correspond to the minimum and maximum 3σ values for DWK 3). Then a fitted normal distribution (depicted by the orange line) was plotted over the actual energy data using the mean and standard deviation of DWK 3. The normal distribution plotted shows the range of 99.7% of the DWK 3 power measurements.

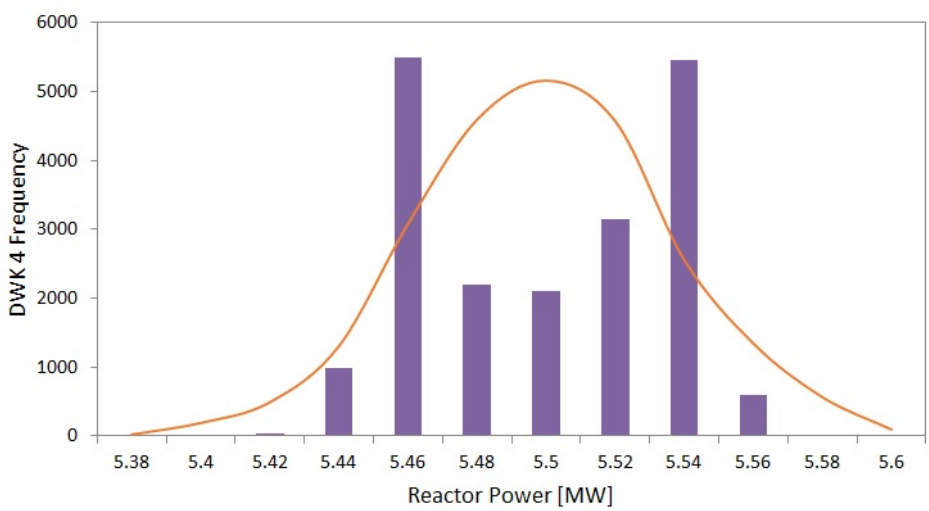

Figure 7.3: The steady-state power detected by DWK 4 from minute 10000 to 30000 during the 10-13-17 to 12-19-17 operation period was grouped into energy power intervals of 0.02 MW from 5.38 MW to 5.6 MW (which correspond to the minimum and maximum 3σ values for DWK 4). Then a fitted normal distribution (depicted by the orange line) was plotted over the actual energy data using the mean and standard deviation of DWK 4. The normal distribution plotted shows the range of 99.7% of the DWK 4 power measurements.

The percent discrepancy between DWK channels 1-4 and thermal power was determined

from steady-state operation data over 16 days from 09-09-17 to 09-25-17. The percent discrepancy for DWK's 2, 3, and 4 was plotted against time with the corresponding shim bank heights also included. These plots are shown in Figures 7.4, 7.5, and 7.6 below.

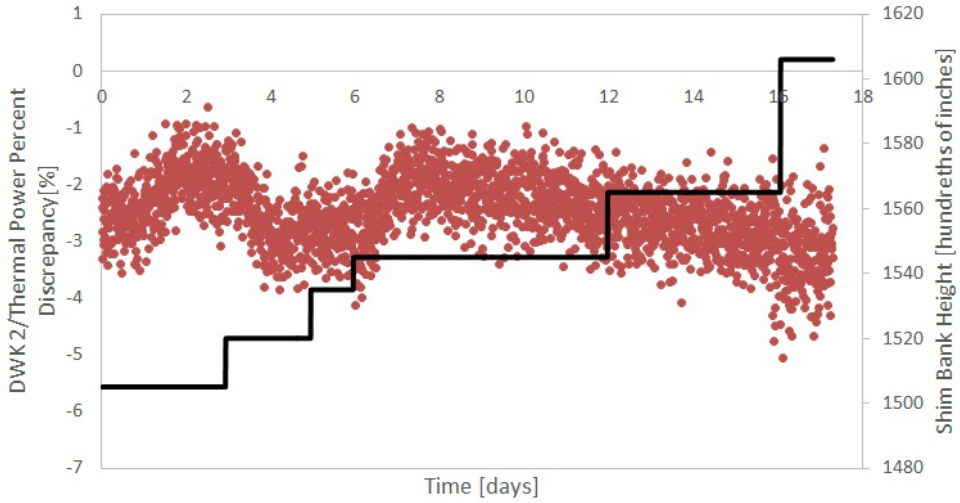

Figure 7.4: The percent discrepancy between DWK 2 and thermal power during steady-state operation is plotted every ten minutes over 16 days from 09-09-17 to 09-25-17. This plot is overlaid with a black line representing the shim bank height over the same time frame. The percent discrepancy seems to drift downwards from day 8 to day 16.

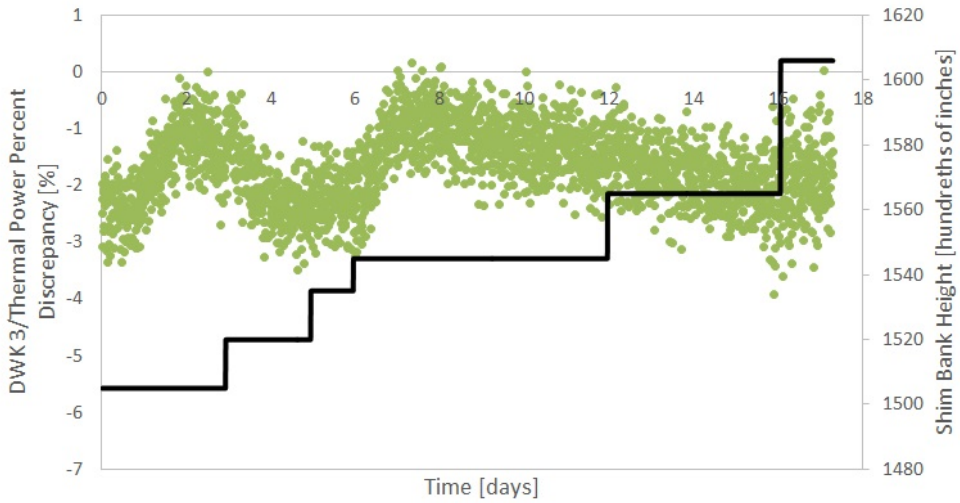

Figure 7.5: The percent discrepancy between DWK 3 and thermal power during steady-state operation is plotted every ten minutes over 16 days from 09-09-17 to 09-25-17. This plot is overlaid with a black line representing the shim bank height over the same time frame. The percent discrepancy seems to drift downwards from day 8 to day 16.

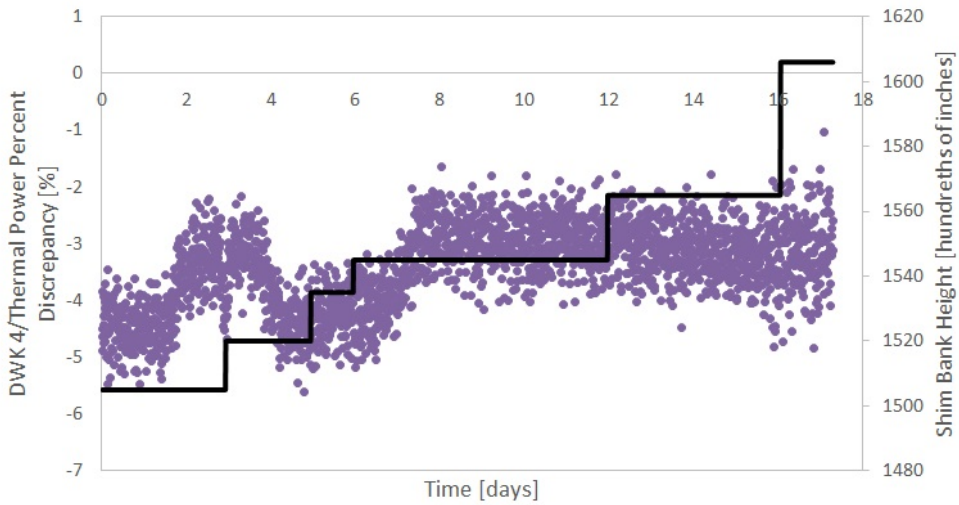

Figure 7.6: The percent discrepancy between DWK 4 and thermal power during steady-state operation is plotted every ten minutes over 16 days from 09-09-17 to 09-25-17. This plot is overlaid with a black line representing the shim bank height over the same time frame. The percent discrepancy seems to drift downwards from day 8 to day 16.

The same analysis was performed for DWK channels 1-4 on steady-state operation data over 28 days from 10-16-17 to 11-13-17. The percent discrepancy plots for DWK's 2, 3, and 4 are shown in Figures 7.7, 7.8, and 7.9 below.

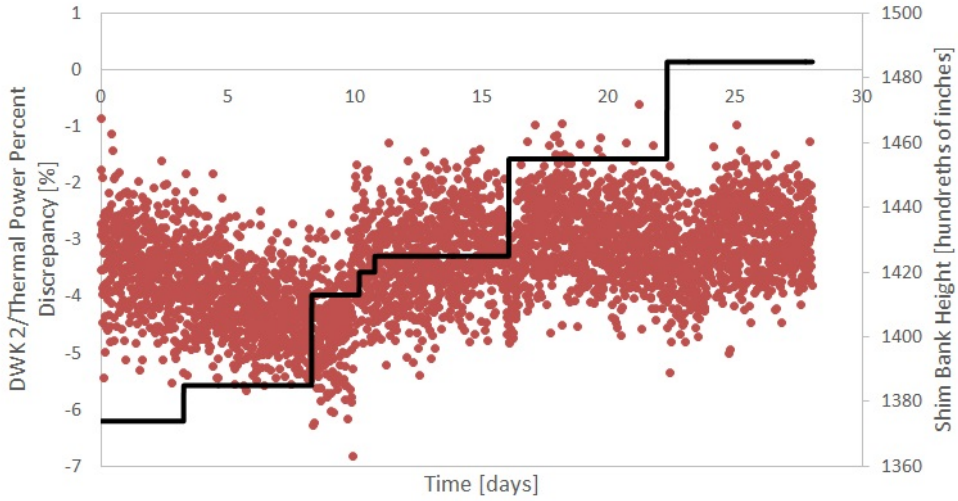

Figure 7.7: The percent discrepancy between DWK 2 and thermal power during steady-state operation is plotted every ten minutes over 28 days from 10-16-17 to 11-13-17. This plot is overlaid with a black line representing the shim bank height over the same time frame. The percent discrepancy seems to drift downwards from day 15 to day 28.

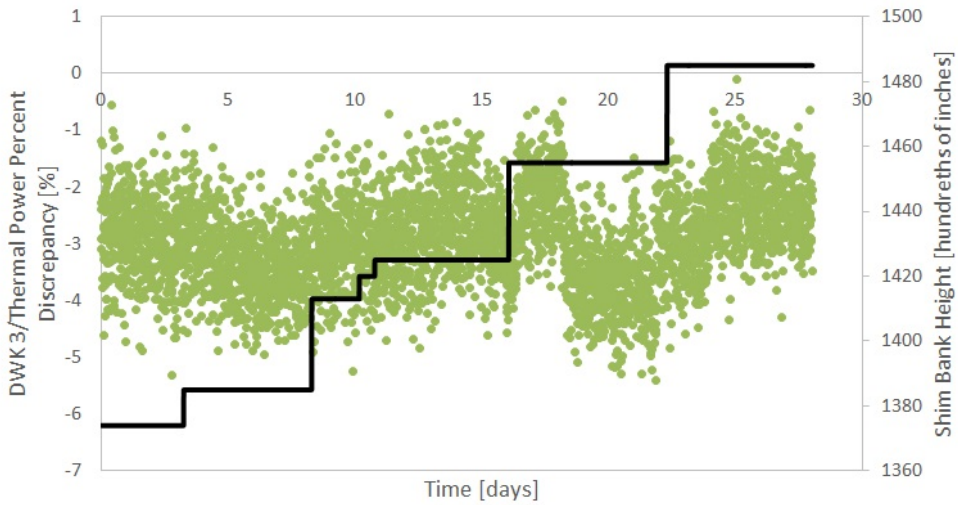

Figure 7.8: The percent discrepancy between DWK 3 and thermal power during steady-state operation is plotted every ten minutes over 28 days from 10-16-17 to 11-13-17. This plot is overlaid with a black line representing the shim bank height over the same time frame. The percent discrepancy seems to drift downwards from day 15 to day 28.

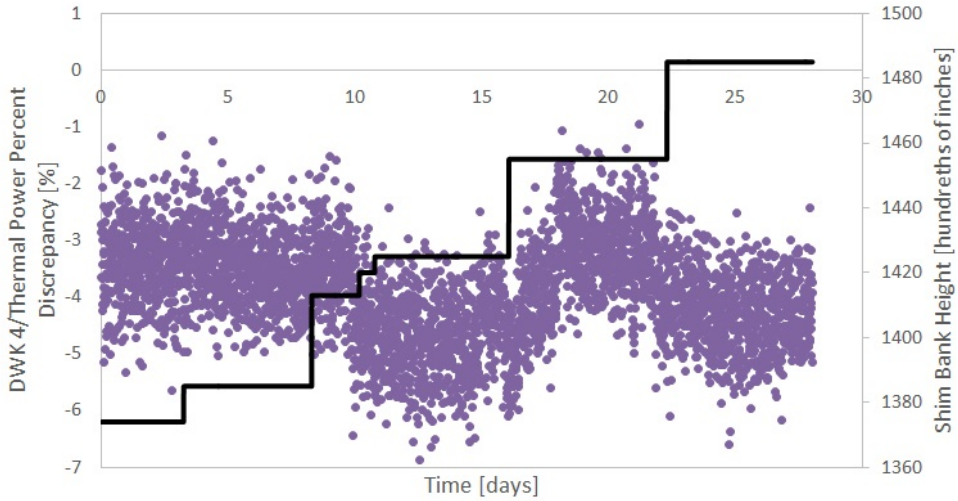

Figure 7.9: The percent discrepancy between DWK 4 and thermal power during steady-state operation is plotted every ten minutes over 28 days from 10-16-17 to 11-13-17. This plot is overlaid with a black line representing the shim bank height over the same time frame. The percent discrepancy seems to drift downwards from day 15 to day 28.

Bibliography

[1] J. Deutch, "Update to the mit 2003 future of nuclear power: An interdisciplinary mit study," 2009.

[2] N. R. Comission. (Mar. 2015). Nuclear reactor safety research, [Online]. Available: https://www.nrc.gov/about-nrc/regulatory/research/reactor-rsch.html#plant.

[3] N. R. Laboratory. (2017). "the reactor at mit", [Online]. Available: https://nrl.mit.edu/reactor.

[4] U. S. R. Commission, "Background on research and test reactors," Aug. 2015.

[5] *Mit research reactor (mitr-ii) technical specifications*, For License Issued by Nuclear Regulatory Commission, MIT Nuclear Reactor Laboratory, Nov. 2010.

[6] *Facility description manual*, Nuclear Reactor Laboratory, Sep. 2014, ch. 5 Nuclear Instrumentation Systems.

[7] *Facility description manual*, Nuclear Reactor Laboratory, Sep. 2014, ch. 4 Reactor Control System.

[8] *Lar - nss upgrade*, NRL, NRL, 2014.

[9] *Reactor protection system (rps)*, IAEA, Dec. 2004, ch. 5.4 Fission chambers.

[10] *Neutronics electronics lab*, Tarleton State University, 2015.

[11] *Facility description manual*, Nuclear Reactor Laboratory, Sep. 2014.

[12] M. O. Team, "Dwk full power startup 5-5-17 to 5-22-17."

[13] G. F. Knoll, *Radiation Detection and Measurement: Third Edition*. Ann Arbor, MI: John Wiley & Sons, Inc., 2000.

[14] e. a. A. Abebe, *Statistics and Data Analysis*. Kalamazoo, MI: Western Michigan University, 2001.

[15] D. K. Sun, "Memo for neutron flux at 3gv and 4th ports," Cambridge, MA, Jan. 2018.